Pharmacology Profiles of ALK and FLT3 Kinase Inhibitors against Non-Small-Cell Lung Cancer Cells and Acute Myeloid Leukemia Cells with Cancer Driver Mutations

January 2019

Masamichi MORI

Pharmacology Profiles of ALK and FLT3 Kinase Inhibitors against Non-Small-Cell Lung Cancer Cells and Acute Myeloid Leukemia Cells with Cancer Driver Mutations

A Dissertation Submitted to

the Graduate School of Life and Environmental Sciences,

the University of Tsukuba

in Partial Fulfillment of the Requirements

for the Degree of Doctor of Philosophy in Biological Science

(Doctoral Program in Biological Sciences)

Masamichi MORI

Table of Contents

Abstract

Gene mutation and genomic abnormality are the characteristics of cancer leading to aberrant cell growth. Tumors accumulate abnormalities during their somatic evolution of life and acquire intra-tumor heterogeneity. When malignant cells obtain a driver mutation or genetic alteration on oncogene or tumor suppressor gene, their feature becomes more aggressive and dominant in tumor tissues. In the studies described here, I focused on a fusion kinase of echinoderm microtubule associated protein like 4 (EML4) and anaplastic lymphoma receptor tyrosine kinase (ALK), EML4-ALK, and further Fms-like tyrosine kinase 3 (FLT3) with constitutively active mutation, which are driver mutations in a subset of non-small cell lung cancer (NSCLC) and acute myeloid leukemia (AML), respectively. For both tumor types, their kinase inhibitors, ASP3026 and gilteritinib were investigated to elucidate their basic profiles as anticancer drug candidates prior to initiation of each clinical trial. In addition, revealing the roles of both aberrant kinases in cancer biology was also aimed for the studies.

In the first part, ASP3026 was characterized in NSCLC cells with EML4-ALK. ASP3026 inhibited ALK activity in an ATP-competitive manner. In mice xenografted with NCI-H2228 cells expressing EML4-ALK, orally administered ASP3026 was well absorbed in tumor tissues, reaching concentrations >10-fold higher than those in plasma, and induced tumor regression with a wide therapeutic margin between efficacious and toxic doses. ASP3026 also showed potent antitumor activities, including tumor

shrinkage to a non-detectable level, in *hEML4-ALK* transgenic mice and prolonged survival in mice with intrapleural NCI-H2228 xenografts. In an intra-hepatic xenograft model using NCI-H2228 cells, ASP3026 induced continuous tumor regression, whereas mice treated with crizotinib showed tumor relapse after an initial response. Finally, ASP3026 exhibited potent antitumor activity against cells expressing EML4-ALK with a mutation in the gatekeeper position (L1196M) that confers crizotinib resistance. Taken together, these findings indicate that ASP3026 has potential efficacy for NSCLC and is expected to improve the therapeutic outcomes of cancer patients with ALK abnormality.

In the second part, gilteritinib was characterized in AML cells with FLT3 active mutation. Initial kinase studies showed that gilteritinib, a type I tyrosine kinase inhibitor, was highly selective for both FLT3 and AXL while having weak activity against c-KIT. Gilteritinib demonstrated potent inhibitory activity against the internal tandem duplication (FLT3-ITD) and FLT3-D835Y point mutations in cellular assays using MV4-11 and MOLM-13 cells as well as Ba/F3 cells expressing mutated FLT3. Gilteritinib also inhibited FLT3-F691 mutations, although to a lesser degree, in these assays. Furthermore, gilteritinib decreased the phosphorylation levels of FLT3 and its downstream targets in both cellular and animal models. *In vivo*, gilteritinib was distributed at high levels in xenografted tumors after oral administration. The decreased FLT3 activity and high intratumor distribution of gilteritinib translated to tumor regression and improved survival in xenograft and intra-bone marrow transplantation models of FLT3-driven

AML. No overt toxicity was seen in mouse models treated with gilteritinib. These results indicate that gilteritinib may be an important next-generation FLT3 inhibitor for use in the treatment of FLT3 mutation-positive AML.

In the pharmacology studies with ASP3026, it selectively inhibited ALK activity and showed an antitumor efficacy against tumor cells harboring EML4-ALK. ASP3026 also showed its efficacy against cells resistant to another ALK inhibitor. In the studies with gilteritinib, it selectively inhibited FLT3 sparing c-KIT and prolonged survival in an animal model with AML cells harboring of active mutation of FLT3. From these results, I revealed the attractive pharmacology profiles of both compounds that they showed antitumor activity in several models including resistant models to another compound through inhibiting target molecules.

These study results also indicated the dependencies of ALK and FLT3-mutated cells on each driver kinase for their growth and survival. As the sensitivities (inhibitory activities) of each inhibitor differ among cells and animal models tested, it was inferred that several other intra- and extra-cellular factors than driver kinases are also involved in maintenance of tumors. The outcomes of clinical trials for both compounds have been already available. While they showed efficacies in NSCLC and AML patients with driver mutated kinases as expected, the diseases have made progresses with time in many patients. Tumors are not uniform aberrant cells but consist of heterogeneous tumor cells. There are possibilities that minor tumor cells, which are not dependent on driver kinases,

emerged to be prominent, targeted cells acquired additional mutations on the kinases not to be effective to the therapies and/or other alternative signal pathways were activated. In the series of experiments, I partly revealed the roles of both driver kinases in tumors, which would lead to further understanding of cancer biology toward concurring cancer.

Abbreviations

ALK	anaplastic lymphoma ceceptor tyrosine kinase
AML	acute myeloid leukemia
ATCC	American Type Culture Collection
AUC	area under the plasma concentration–time curve
BLI	bioluminescent imaging
C_{max}	maximum plasma concentration
CML	chronic myeloid leukemia
CT	computed tomography
EGFR	epidermal growth factor receptor
EML4	echinoderm microtubule associated protein like 4
FLT3	fms-like tyrosine kinase 3
IBMT	intra-bone marrow transplantation
IC_{50}	half maximal inhibitory concentration
ITD	internal tandem duplication
KIF5B	kinesin family member 5B
MSA	mobility shift assay
NSCLC	non-small cell lung cancer
PD-1	programmed cell death 1
PDB	Protein Data Bank
TBS-T	tris buffered saline tween-20
TFG	tropomyosin receptor kinase (TRK)-fused gene
TK	tyrosine kinase
TKI	tyrosine kinase inhibitor
TKD	tyrosine kinase domain
T_{max}	time to reach maximum plasma concentration

General Introduction

Cancer is one of the major causes of mortality in the world. In Japan, more than 300,000 people die of cancer in a year, which accounts for around 30% of all cases according to the Vital Statistics issued by Ministry of Health, Labour and Welfare in 2016 (1). What are the differences between normal cells and malignant cells? One of the characteristics of cancer is aberrant cell growth resulting from gene mutation and/or genomic abnormality (2-4). Malignant cells suppress gene repair of aberrant genes and further survive without falling into apoptosis (5). Malignant cells also acquire the ability to escape from immune surveillance (6). Malignant cells sometimes have the potential to metastasize to another region in the same organ and another tissue. When malignant cells disturb the functions of normal tissues, the life of the patient would be threatened, regardless of whether the malignant cells grow in the original place or metastasized places. As such, a variety of aberrances is responsible for each type of cancers as well as each tumor cell.

Gene mutation or genetic alteration is the initial step for cancer development. Tumors accumulate abnormalities during their somatic evolution of life and acquire intra-tumor heterogeneity (7). When malignant cells obtain a driver mutation or genetic alteration on oncogene or tumor suppressor, their feature becomes more aggressive and dominant in tumor tissues. Other passenger mutations they probably have would further contribute to support the tumor development of dominant malignant cells.

There are many evidences showing that a cancer driver mutation or genetic alteration is a key to tumor development for certain types of cancers. For example, the driver tyrosine kinase BCR-ABL, which is a fusion protein of BCR and ABL, is implicated in the pathogenesis of chronic myeloid leukemia (CML), and imatinib, an inhibitor of BCR-ABL, induces hematological and cytogenetic responses that help prevent disease progression (8, 9). In CML, the Philadelphia chromosome as a hallmark is resulting from a reciprocal translocation between the long arms of chromosomes 9 and 22. The resulting fusion protein, BCR-ABL, is constitutively active tyrosine kinase that can transform myeloid progenitor cells and drives the development of CML. Cancer drivers, which could be molecular targets of therapies, are also found in solid malignancies and the targeted therapies have proved effective against them, such as the use of trastuzumab against HER2 in breast cancer (10), gefitinib and erlotinib against epidermal growth factor receptor (EGFR) in NSCLC (11-13), and vemurafenib against BRAF V600E in melanoma (14). In the EGFR and BRAF cases, a point mutation of each receptor makes the tyrosine kinase to be constitutively active and promotes the development of tumors. These mutated receptors become oncogenes. In the HER2 case, its overexpression or amplification contributes to the dependency of the tumor cells to the growth signal.

Regarding research and development of cancer drugs, kinase inhibitors are attractive therapeutics against cancer with specific driver mutations (15). The targets are druggable and the high efficacies are expected due to their dependency on the kinase activities for

the growth and survival. In addition, the inhibitors would be strong tools for understanding cancer biology. Firstly, in the discovery stage of drugs, it should be investigated whether the inhibitors can inhibit the cancer cell growth and induce cell death *in vitro*. It is also important to confirm the inhibition of target kinase and the downstream signal transduction in target cells. The inhibitors should be well absorbed, if oral application is desired, and be importantly well tolerated in animals. From a set of experiments using cell lines with driver mutations, one can know whether the inhibitors have a potential to be effective against cancers with the target mutations and confirm the dependency of the cells on the mutations at least in the non-clinical conditions.

Cancer biology in real patients would be more complex and the situation of tumor cells would differ by patients and even among tumors in the same patient (7). In addition to diversity of malignant cells in their abnormalities, their microenvironments such as growth environment, oxygen/energy conditions, and interaction with stromal cells, also differ among cells which causes cancer biology to be further complex. In the case of CML, most patients well responded to the ABL inhibitors and the efficacies lasted for a long time (9). The patients can even expect to become cured. The complexity and heterogeneity of CML is thought to be lower compared to solid tumors, where the efficacy is usually partial and tentative and the relapse will happen roughly 10 to 12 months after the tumor shrinkage in median (10-14, 16-18). In the case of relapse, tumor cells usually have additional mutations to evade the inhibitors' efficacy. The mutations

are often found in another position of the kinase for which the inhibitor shows weaker activity and/or in another kinase which can activate the downstream of the original target kinase. In other cases, another clone could be dominant instead of the original clone. Cancer dynamically evolves in its biological properties also with the treatment.

In the studies described in this dissertation, I revealed the basic profiles of ALK inhibitor ASP3026 against ALK-mutated NSCLC and FLT3/AXL inhibitor gilteritinib against FLT3-mutated acute myeloid leukemia in non-clinical settings to elucidate their potentials as anticancer drug candidates prior to initiation of each clinical trial. I also confirmed the driver kinase dependencies of tumor cells in a set of experiments *in vitro* and *in vivo* with aiming to reveal the roles of both aberrant kinases in cancer biology. These inhibitors could be useful tools to elucidate cancer biology through non-clinical, clinical, and the mixed approaches in future.

Part I

The selective anaplastic lymphoma receptor tyrosine kinase inhibitor ASP3026 induces tumor regression and prolongs survival in non-small cell lung cancer model mice

Abstract

Activation of anaplastic lymphoma receptor tyrosine kinase (ALK) is involved in the pathogenesis of several carcinomas, including non-small cell lung cancer (NSCLC). Echinoderm microtubule associated protein like 4 (EML4)-ALK, which is derived from the rearrangement of *ALK* and *EML4* genes, has been validated as a therapeutic target in a subset of NSCLC patients. Here, my colleagues and I investigated the effects of ASP3026, a novel small molecule ALK inhibitor, against ALK-driven NSCLC. ASP3026 inhibited ALK activity in an ATP-competitive manner and had an inhibitory spectrum that differed from that of crizotinib, a dual ALK/MET inhibitor. In mice xenografted with NCI-H2228 cells expressing EML4-ALK, orally administered ASP3026 was well absorbed in tumor tissues, reaching concentrations >10-fold higher than those in plasma, and induced tumor regression with a wide therapeutic margin between efficacious and toxic doses. In the same mouse model, ASP3026 enhanced the antitumor activities of paclitaxel and pemetrexed without affecting body weight. ASP3026 also showed potent antitumor activities, including tumor shrinkage to a non-detectable level, in *hEML4-ALK* transgenic mice and prolonged survival in mice with intrapleural NCI-H2228 xenografts. In an intra-hepatic xenograft model using NCI-H2228 cells, ASP3026 induced continuous tumor regression, whereas mice treated with crizotinib showed tumor relapse after an initial response. Finally, ASP3026 exhibited potent antitumor activity against cells expressing EML4-ALK with a mutation in the

gatekeeper position (L1196M) that confers crizotinib resistance. Taken together, these findings indicate that ASP3026 has potential efficacy for NSCLC and is expected to improve the therapeutic outcomes of cancer patients with ALK abnormality.

Introduction

Lung cancer is the most commonly diagnosed cancer and the leading cause of cancer death worldwide (19). Treatment outcomes with conventional antitumor drugs in advanced or metastatic non-small-cell lung cancer (NSCLC) remain unsatisfactory due to low rates of response and long-term survival (20). However, in the last few decades, investigations of the molecular mechanisms of cancer pathogenesis have identified several cancer drivers, such as receptor tyrosine kinases (TKs), which have been used for new, targeted therapies against several types of cancers, including NSCLC (8-13). Such therapies have markedly improved response rates and survival outcomes of cancer patients, and represent a paradigm shift in cancer treatment. For example, the driver TK BCR-ABL is implicated in the pathogenesis of chronic myeloid leukemia, and imatinib, an inhibitor of BCR-ABL, induces hematological and cytogenetic responses that help prevent disease progression (8, 9). Targeted therapies against cancer drivers have also proved effective against solid malignancies, such as the use of trastuzumab against HER2 in breast cancer (10), gefitinib and erlotinib against epidermal growth factor receptor (EGFR) in NSCLC (11-13), and vemurafenib against BRAF V600E in melanoma (14).

EML4-ALK is a fusion gene comprising portions of the echinoderm microtubule associated protein like 4 (*EML4*) and anaplastic lymphoma kinase (*ALK*) genes, and was first found in a subset of NSCLC cells (21, 22). Soda and colleagues (21) discovered *EML4-ALK* by screening a retroviral complementary DNA expression library generated

from a lung adenocarcinoma specimen surgically resected from a 62-yr-old man with a smoking history. *EML4-ALK* was formed through disruption of *EML4* at a position ~3.6-kb downstream of exon 13 and ligation to a position 297-bp upstream of exon 21 of *ALK*. EML4–ALK has transforming potential that is dependent on its kinase activity, while the coiled-coil domain of EML4 mediates the constitutive dimerization and cytoplasmic activation of EML4-ALK, which together are responsible for the generation of transformed cell foci *in vitro* and tumor formation in nude mice (21). Separately, Rikova and colleagues (22) discovered a variant of EML4-ALK, in which intron 6 of *EML4* is fused to the *ALK* gene, and another ALK fusion protein, TRK-fused gene (TFG)-ALK, during phosphoproteomic analyses of tyrosine signaling. More recently, Takeuchi and colleagues (23) identified a novel oncokinase fusion protein, kinesin family member 5B (KIF5B)-ALK, using an immunohistochemistry-based diagnostic system. The identification of these various ALK-fusion proteins indicates that the kinase activity of ALK plays an important role in the pathogenesis of a subset of NSCLC. In addition, treatment of spontaneous pulmonary tumor in *hEML4-ALK* transgenic mice with an ALK inhibitor or repression of ALK expression results in tumor regression (24, 25). Together, these experimental evidences suggest that EML4-ALK is a targetable genetic lesion in NSCLC (26).

ALKoma, tumors carrying abnormal ALK as an essential growth driver, have also been found in several cancer types other than NSCLC (27). In these tumor cells, ALK is

rendered oncogenic as a result of its fusion to various proteins, including nucleophosmin (nucleolar phosphoprotein B23, numatrin) in anaplastic large cell lymphoma (28), tropomyosin 3 or 4 in inflammatory myofibroblastic tumors (29), vinculin in renal medullary carcinoma (30, 31), and clathrin in ALK-positive diffuse large B-cell lymphoma (32). In addition, activated mutation of ALK is also involved in the development of neuroblastoma and anaplastic thyroid cancer (33, 34). Several ALK inhibitors with efficacy against ALKoma in preclinical models and patients have been identified (35-38). For example, the small-molecule ALK and MET inhibitor crizotinib exhibited high efficacy with overall response rates of ≥50% in clinical trials of NSCLC patients harboring an EML4-ALK oncogenic kinase (16, 17). However, the treatment was not curative, and the patients developed resistance in target lesions and/or metastatic sites and had a progression free survival of only approximately 10 months (16-18). Two secondary point mutations (L1196M and C1156Y) have been identified within the kinase domain of EML4-ALK in tumor cells isolated from a patient who relapsed after an initial response to crizotinib (39). The point mutation L1196M is analogous to other kinase domain mutations, including the T790M mutation in EGFR (40) and T315I mutation in BCR-ABL (41), in gatekeeper positions seen in patients who developed resistance to tyrosine kinase inhibitor (TKI) treatment (41). The gatekeeper position including the L1196M mutation site is located at the bottom of the ATP-binding pocket of EML4-ALK, and the presence of an amino acid with a bulky side chain at this position interferes with

the interaction of the TKI with the kinase domain of the target protein, thereby decreasing the efficacy of treatment (42). Thus, more potent ALK inhibitors, such as those capable of inhibiting L1196M ALK, are needed to overcome the resistance that often develops in both lung and metastatic sites.

In the present study, my colleagues and I characterized a recently discovered novel and selective small molecule ALK inhibitor, ASP3026, against ALK-driven NSCLC tumors in a non-clinical setting to elucidate the potential as an anticancer drug candidate prior to initiation of the clinical trial and also to reveal the role of the aberrant kinase in cancer biology. My colleagues and I examined the inhibitory effects of ASP3026 against ALK in cell-free systems and cellular assays, and evaluated the antitumor activity and survival benefits of ASP3026 in mouse models with ALK-driven tumors in lung and metastatic sites. In addition, my colleagues and I also evaluated the antitumor activity of ASP3026 against cells expressing EML4-ALK with a mutation in the gatekeeper position and in combination with conventional antitumor agents in mouse models of NSCLC.

Materials and Methods

Compounds, cell lines, and antibodies

ASP3026 (43) and crizotinib were synthesized by Astellas Pharma Inc. (Tokyo, Japan). Paclitaxel and pemetrexed were purchased from LC laboratories (Woburn, MA, USA), and carboplatin was obtained from Bristol-Myers Squibb (New York, NY, USA). NCI-H2228 cells were purchased from the American Type Culture Collection (ATCC, Manassas, VA, USA) in July 2007 and authenticated by Short Tandem Repeat profiling (Cell ID, Promega). H2228-luc cells, which exogenously express firefly luciferase, were prepared at Astellas Pharma Inc. 3T3 cells were obtained from the ATCC in June 2007 (not authenticated) and were engineered to express either wild-type (EML4-ALK/3T3) or L1196M-mutated EML4-ALK (L1196M/3T3). Antibodies to ALK (C26G7), phosphorylated ALK (Tyr1604), p44/42 MAPK (Erk1/2), Phospho-p44/42 MAPK (Erk1/2) (Thr202/Tyr204) (197G2), Phospho-Stat3 (Tyr705), Akt, and Phospho-Akt (Ser473) (193H12) were purchased from Cell Signaling Technology, Inc. (Beverly, MA, USA). Anti-actin antibody A2066 was purchased from Sigma-Aldrich Co. (St. Louis, MO, USA).

Kinase inhibitory assays

EML4-ALK variant 1 kinase and its L1196M-mutated form were isolated from Ba/F3 cells transformed with the respective forms of EML4-ALK. Kinase activity was measured with HTRF® KinEASE™-TK (SCETI Medical Labo K.K., Tokyo, Japan) in

the presence of various concentrations of ASP3026 or crizotinib.

An inhibitory assay for a panel of 86 TKs (Table 1) was conducted using ATP concentrations that were approximately equal to the Km value for each kinase using a TK-ELISA or Off-chip Mobility Shift Assay (MSA) at Carna Biosciences, Inc. (Kobe, Japan). The inhibitory percentage of ASP3026 and crizotinib against kinase activity was first determined at concentrations of 100 and 1000 nM in a single experiment. Half maximal inhibitory concentration (IC_{50}) values were then separately determined in the presence of various concentrations of each compound in three individual experiments.

Anti-proliferative assays

NCI-H2228 cells were plated in RPMI 1640 supplemented with 10% heat-inactivated FBS in 96-well Sumilon cell-tight spheroid plates (Sumitomo Bakelite, Tokyo, Japan) at 2000 cells/well and then incubated at 37°C in a 5% CO_2 atmosphere overnight. The cells were exposed to test compounds, which were dissolved in DMSO as a solvent, for 5 days, and viable cell numbers were then determined using the CellTiter-Glo™ Luminescent Cell Viability Assay (Promega, Madison, WI, USA). The IC_{50} value of each compound was calculated by nonlinear regression analysis using the Sigmoid-Emax model, and the mean IC_{50} values were calculated from four individual experiments. In the assay with 3T3 cells, the cells were plated in DMEM supplemented with 10% heat-inactivated FBS in 96-well spheroid plates (Sumitomo Bakelite) at 500 cells/well, incubated overnight, and then treated with the test compounds for 2 days. The IC_{50} values were determined

from a single experiment.

Immunoblotting

NCI-H2228 cells were seeded at 4 to 5×10^5 cells/well in 12-well HydroCell™ plates (CellSeed, Tokyo, Japan), incubated for 2 days, and ASP3026 was then added to each well at a final concentration of 0 (DMSO), 10, 100, or 1000 nM. Cell lysates were prepared for immunoblot analysis of EML4-ALK, ERK, STAT3, AKT, and actin after 4 h of ASP3026 treatment. In an *in-vivo* experiment, mice with NCI-H2228 tumors were treated with ASP3026 at a single oral dose of 10 mg/kg, and tumors were then excised 4 h after administration.

The lysates from cell and tumor samples were separated by electrophoresis and then transferred onto nitrocellulose membranes. After blocking with Blocking One or Blocking One-P (Nacalai Tesque, Kyoto, Japan) for 1 h, each membrane was incubated with anti-ALK, anti-phospho-ALK, anti-ERK, anti-phospho-ERK, anti-phospho-STAT3, anti-AKT, or anti-phospho-AKT antibodies overnight at 4°C. The membranes were washed with 1×tris buffered saline tween-20 (TBS-T, Thermo Fisher Scientific Inc., Rockford, IL, USA) and then incubated with anti-rabbit IgG HRP-linked antibody (Cell Signaling Technology) for 1 h at room temperature. After a final washing, ECL Western Blotting Detection Reagents (GE Healthcare, Chalfont St. Giles, UK) were applied to the membranes, and signals were detected with a CCD camera (AISIN, Aichi, Japan) and quantified using a LumiVision PRO 400EX system (Taitec, Saitama, Japan) or

ImageJ software (NIH, Bethesda, MD, USA). The mean percentage of phosphorylated protein/total protein relative to that in vehicle-treated cells was then calculated.

***In-vivo* models**

All animal experimental procedures were approved by the Institutional Animal Care and Use Committee of Astellas Pharma Inc. Furthermore, Astellas Pharma Inc., Tsukuba Research Center was awarded Accreditation Status by AAALAC International. ASP3026 and crizotinib in a 0.5% methylcellulose solution were administered orally at once or twice daily doses starting after confirming tumor growth in each experiment. NCI-H2228 cells were subcutaneously inoculated into the flank of male NOD-SCID mice (NOD.CB17-Prkdcscid/J, Charles River Laboratories Japan, Inc., Kanagawa, Japan) at 5×10^6 cells/0.1 mL/mouse. EML4-ALK/3T3 and EML4-ALK L196M/3T3 cells were subcutaneously inoculated into the flank of the male nude mice (CAnN.Cg-Foxn1nu/CrlCrlj[nu/nu], Charles River Laboratories Japan, Inc.) at 3×10^6 cells/0.1 mL/mouse. Tumor diameter was measured using a caliper and tumor volume was determined by calculating the volume of an ellipsoid using the formula: length × width^2 × 0.5.

In an intrapleural xenograft model, H2228-luc cells were directly inoculated at 1×10^5 cells/20 μL/mouse into the pleural cavity of male NOD/SCID mice under anesthesia with isoflurane. In an intra-hepatic xenograft model, H2228-luc cells were directly inoculated into the portal vein of male NOD/SCID mice at 1×10^6 cells/100 μL/mouse. Tumor

growth was monitored by bioluminescent imaging (BLI) of the chest and abdominal areas with an IVIS Spectrum Imaging System (Caliper Life Sciences, Hopkinton, MA). The survival of mice was monitored daily.

hEML4-ALK transgenic mice were provided by Jichi Medical University (Tochigi, Japan) and were generated as previously described (24). Briefly, a complementary DNA fragment encoding EML4-ALK variant 1 was ligated to the surfactant protein C promoter and then injected into pronuclear-stage embryos of C57BL/6J mice. The tumors were monitored by computed tomography (CT) scan, which was performed for approximately 5 min under anesthesia induced with 2.5% isoflurane using an Inveon CT (Siemens, Munich, Germany). Data reconstruction and analysis were performed using Inveon Acquisition Workplace software (Siemens). Volumes of interests were manually drawn for pulmonary tumors detected in the CT images.

Pharmacokinetics

NOD-SCID mice subcutaneously xenografted with NCI-H2228 cells received a 5-day repeated oral dosing of 1, 3, and 10 mg/kg ASP3026 suspended in a 0.5% methylcellulose solution. Blood samples were collected from the inferior vena cava using a heparinized syringe, and plasma samples were prepared by centrifugation. Tumor samples were also collected from each mouse, and tumor weight was measured. The plasma and tumor concentrations of ASP3026 were measured using high-performance liquid chromatography-tandem mass spectrometry at Toray Research Center, Inc.

(Kanagawa, Japan). Maximum plasma concentration (C_{max}), time to reach maximum plasma concentration (T_{max}), and area under the plasma concentration–time curve from time 0 h to 24 h ($AUC_{0\text{-}24h}$) were calculated from the mean concentrations of ASP3026 using WinNonlin Professional V6.1 (Pharsight, Mountain View, CA, USA).

Computational modeling

As the X-ray structures of both wild-type ALK and the L1196M variant of ALK with crizotinib (PDB ID: 2XP2 and 2YFX) are publicly available, computation models of crizotinib were generated by adding missing hydrogen atoms and minimizing the coordinates of hydrogen atoms using MOE (Chemical Computing Group Inc., Montreal, Quebec, Canada). Docking simulation of ASP3026 with wild-type ALK was performed using the docking software GLIDE (Schrodinger, LLC, New York, NY, USA). Wild-type ALK with NVP-TAE684 (PDB ID: 2XB7) was used as a template for the docking, and hydrogen atoms were added using MOE. The docking mode with the highest docking score was employed in the modeling. The binding model of ASP3026 and ALK L1196M was generated by superimposing the backbone atoms of the protein coordinates over those of the 2YFX structure. All of the figures showing X-ray structures and docking results were constructed using MOE.

Results

ASP3026 inhibits the growth of ALK-dependent cells

ASP3026 was identified through a medicinal chemistry campaign (Fig. 1A) designed to obtain compounds with different profiles from a reported ALK inhibitor (43, 44). The kinase selectivity of ASP3026 was evaluated and compared with that of crizotinib against a panel of 86 TKs (Table 1). ASP3026 inhibited 11 TKs by more than 50% at 1000 nM, and had the highest selectivity for ALK, ROS, and ACK kinases (Table 2). The kinase selectivity of ASP3026 clearly differed from that of crizotinib. Specifically, ASP3026 was more selective for FRK, YES, ACK, TNK1, and EGFR (L858R) among all tested kinases, whereas crizotinib had higher selectivity for MET, RON, LCK, JAK2, MUSK, TRKs, TYRO3, AXL, MER, and EPHs.

My colleagues and I next evaluated the anti-proliferative activity of ASP3026 against NCI-H2228 NSCLC cells endogenously expressing EML4-ALK variant 3 using a spheroid cell culture system. After 5 days of treatment, ASP3026 inhibited the growth of NCI-H2228 cells with an IC_{50} value of 64.8 nM (Fig. 1B). This value was higher than the concentration of ASP3026 required to achieve comparable results in the kinase inhibitory assays, and may possibly have been due to a higher ATP concentration in the NCI-H2228 NSCLC cells than that used in the assay. The growth suppression was accompanied by inhibition of ALK phosphorylation in the cells, in which the levels of phosphorylated ALK were 70%, 40%, and 9% after 4-h treatment with 10, 100, and 1000

nM ASP3026, respectively, compared to the vehicle-treated control cells (Fig. 1C). In addition, ASP3026 treatment also resulted in suppression of phosphorylation of AKT, ERK, and STAT3 at 100 and 1000 nM (Fig. 1C and Table 3).

ASP3026 induces shrinkage of ALK-dependent NSCLC tumors

My colleagues and I next evaluated the antitumor activity of ASP3026 in a NCI-H2228 subcutaneous xenograft mouse model by examining the inhibitory effect of ASP3026 on ALK phosphorylation. A significant (approximately 20%; $p<0.001$) decrease in phosphorylated ALK was observed 4 h after a single oral administration of 10 mg/kg ASP3026 (Fig. 2A). In this model, once-daily oral administration of ASP3026 at 1, 3, 10 and 30 mg/kg/day for 2 weeks dose-dependently inhibited the growth of NCI-H2228 tumors by 69%, >100%, >100%, and >100%, respectively, and induced tumor regression by 0%, 4%, 45%, and 78%, respectively (Fig. 2B). Body weight was not affected by treatment with ASP3026 at any dose, even at 100 mg/kg twice daily (bid) (data not shown, Fig. 3).

Consistent with the observed antitumor activity, ASP3026 was well absorbed after oral administration, with higher concentrations detected in tumor tissues than in plasma at each time point. The tumor/plasma ratios were 13 to 19 for Cmax and 19 to 23 for $AUC_{0\text{-}24h}$ (Fig. 2C and Table 4).

To further evaluate the antitumor activity of ASP3026, *hEML4-ALK* transgenic mice

were treated with once-daily oral dosing of ASP3026 for 10 days after tumors were established in lungs. A series of CT scans taken during the treatment period clearly revealed a reduction of the tumor mass, with complete responses detected in 2 of 3 mice on day 7, and 3 of 3 mice on day 11 after the initiation of treatment at 100 mg/kg (Fig. 4). A significant reduction of pulmonary tumor size in mice treated with 30 and 100 mg/kg ASP3026 was observed, as determined by the quantitative analysis of CT images taken on days 7 and 11 (Fig. 2D). The penetration of ASP3026 into tumors of this transgenic mouse model was confirmed by measurement of the drug concentration in tumors, which was over 100-fold higher compared to those in plasma at approximately 24 h after the final dosing (2295 and 8005 ng/g in tumors, 23 and 43 ng/mL in plasma at 10 and 30 mg/kg, respectively).

ASP3026 enhances antitumor activities of paclitaxel and pemetrexed in mice with ALK-dependent NSCLC tumors

The antitumor activity of ASP3026 in combination with several NSCLC drugs was investigated in a subcutaneous NCI-H2228 xenograft model. Paclitaxel at 12 mg/kg induced tumor regression against NCI-H2228 xenografts, and the combination of paclitaxel with ASP3026 at 10 mg/kg caused further significant regression of tumors compared with each single-treatment group (Fig. 5A). Body weight loss was observed in the paclitaxel treatment groups, but by day 21, body weight had returned to the level

at the initiation of treatment and did not significantly differ from control mice. The difference of body weight between the combination and paclitaxel single-treatment groups did not largely change during the experiment. The combination of ASP3026 at 10 mg/kg with pemetrexed at 50 mg/kg was also effective at reducing tumor volume, which was smaller in the combination group than that in each single-treatment group (Fig. 5B). Pemetrexed treatment also induced body weight loss, which was not further induced by ASP3026. In contrast to paclitaxel and pemetrexed, ASP3026 did not enhance the antitumor activity of carboplatin at 60 mg/kg in this model, as the tumor volume of the combination group was similar to that of the ASP3026 single-treatment group throughout the experimental period (Fig. 5C).

ASP3026 prolongs survival in mice with intrapleural xenografts of ALK-dependent NSCLC cells

My colleagues and I conducted antitumor assays for xenograft tumors in the pleural cavity, which is one of the major metastatic sites for NSCLC. H2228-luc cells were directly inoculated into the pleural cavity of mice, and the implanted cells were monitored using BLI of the chest area. The bioluminescent emissions of inoculated mice showed an approximately 100-fold increase during the 40-day period after cell inoculation and disease-related mortality was observed (Fig. 6A and 7). Using this model, my colleagues and I also evaluated and compared the efficacy of once-daily oral dosing

of ASP3026 and crizotinib. Median survival time was 39 days in vehicle-treated control mice and 71 days in crizotinib-treated mice at 30 mg/kg (Fig. 6A). In contrast, no mice receiving ASP3026 treatment at 30 mg/kg died during the 90-day experimental period (Fig. 6A). The mortality effects were accompanied by changes in the bioluminescent emissions, with crizotinib-treated mice at 30 mg/kg showing increased emissions after an initial reduction, whereas ASP3026-induced reduction of emissions at 30 mg/kg continued throughout the experimental period (Fig. 6B). The mean bioluminescent emission in the ASP3026-treated group was significantly lower than that in the crizotinib-treated group, indicating that the ASP3026-treated animals exhibited a lower tumor burden.

ASP3026 shows antitumor efficacy against ALK-dependent NSCLC tumors in liver

As the liver is one of the metastatic sites in crizotinib-treated patients with EML4-ALK positive NSCLC (28), my colleagues and I evaluated the antitumor activity of ASP3026 against tumors in the liver. H2228-luc cells were inoculated into the portal vein of mice, and the implanted cells were monitored using BLI of the upper abdominal area (Fig. 6C). The bioluminescent emissions of inoculated animals decreased during the initial 10 days after inoculation and showed an approximately 100-fold increase during the subsequent 30 days, with tumors forming in entire lobes of the liver (Fig. 8). During the first 10 days of the treatment, crizotinib at 30 mg/kg as a once daily oral dose reduced

the BLI signal intensity to one third of that at the initiation of treatment (3.2×10^8 to 1.1×10^8 photons/sec), but the emission increased between days 10 to 20 (1.1×10^8 to 2.0×10^8 photons/sec), which is a similar finding to that observed in the intrapleural xenograft model (Fig. 6C). In contrast, the emission was reduced to approximately 1/100 of that at the initiation of treatment by 30 mg/kg ASP3026 as a once daily oral dose for 14 days (3.3×10^8 to 4.2×10^6 photons/sec), and reached 7.7×10^5 photons/sec by the end of the 19-day experimental period (Fig. 6C).

ASP3026 induces regression of tumors harboring gatekeeper-residue mutation L1196M of EML4-ALK

Mutations in the ALK kinase domain that confer resistance to crizotinib were previously identified following sequence analysis of tumor cells derived from a pleural effusion of a crizotinib-relapsed patient who experienced disease progression after a partial response (31). One of the mutations, L1196M, was observed at a gatekeeper position, and it was confirmed that crizotinib shows less inhibitory activity against mutated EML4-ALK with L1196M. To assess the inhibitory activity of ASP3026 against mutated EML4-ALK, here, *in-vitro* kinase inhibitory, *in-vitro* anti-proliferative, and *in-vivo* antitumor assays were conducted. ASP3026 inhibited the kinase activities of wild-type and mutated EML-ALKs with IC_{50} values of 10 and 32 nM, respectively, whereas crizotinib displayed 10-fold weaker activity for mutated EML4-ALK compared to wild

type (Table 5A). In the spheroid cell culture system, both compounds concentration-dependently inhibited the growth of 2-day treated cells, and the IC_{50} values showed a similar tendency to the kinase inhibitory activities. The IC_{50} ratios of ASP3026 and crizotinib against L1196M/3T3 cells versus EML4-ALK/3T3 cells were 3.9 and 9.2, respectively (Table 5B). In addition, crizotinib at 100 mg/kg as a once daily oral dose for 4 days showed no efficacy against L1196M/3T3 tumors, but did induce the regression of EML4-ALK/3T3 tumors (Fig. 9A and 9B). In contrast, ASP3026 induced tumor regression at 100 mg/kg in both models (Fig. 9A and 9B), indicating the therapeutic potential of this drug for patients who are resistant/refractory to crizotinib.

To further understand and compare the inhibitory activity of ASP3026 and crizotinib against mutated EML4-ALK with L1196M, computational modeling of the wild-type and L1196M ALK TK domains was performed (Fig. 9C). The modeling revealed that wild-type ALK had sufficient space for crizotinib to fit within the ATP-binding pocket, whereas the L1196M mutation limits the space available for the methyl group at the benzyl position of crizotinib due to the larger side-chain of methionine compared to leucine. In contrast, ASP3026 was well docked with both wild-type and L1196M ALK.

Discussion

The discovery of EML4-ALK as a drug-targetable cancer driver led to the development of the ALK inhibitor crizotinib, which showed high efficacy in clinical trials with NSCLC patients harboring this oncogenic kinase, with overall response rates of ≥50% (16, 17). However, the treatment was not curative, and the patients developed resistance to crizotinib in brain, liver, and lung tissues with a progression free survival of only approximately 10 months (16-18). Therefore, a need exists for the development of novel ALK inhibitors and drug combinations to further improve treatment outcomes.

In the present study, my colleagues and I demonstrated that ASP3026 has growth inhibitory activity that is accompanied by a decrease of phosphorylated ALK in NCI-H2228 ALK-fusion positive NSCLC cells. In mice xenografted with NCI-H2228 cells, ASP3026 showed antitumor activity with a wide therapeutic margin between efficacious and toxic doses. ASP3026 induced tumor regression at oral doses of 3 mg/kg or more, with no apparent toxicity or body weight loss, even at a dose of 100 mg/kg. The broad therapeutic margin of ASP3026 is possibly due to its high uptake in tumors, higher ALK selectivity, and different spectrum of kinase inhibition compared with crizotinib. In the *hEML4-ALK* transgenic mouse model, ASP3026 also showed potent antitumor activity, as assessed by tumor shrinkage in the lung to non-detectable levels in CT scans. Notably, however, ASP3026 at 10 mg/kg did not induce tumor regression in this model, possibly due to differences in the rate of tumor growth and/or ALK dependency between *hEML4-*

ALK transgenic mice and NCI-H2228 xenografted mice. This finding was also supported by the higher concentration of orally administered ASP3026 in the lung compared with plasma. In a preliminary study of anti-proliferative assays using 145 types of NSCLC-derived cell lines, only 5 cell lines with ALK fusions, including NCI-H2228 and H3122, were sensitive (>50% inhibition at 300 nM) to ASP3026 (data not shown), indicating this compound has selective inhibitory activity against ALK-dependent cancer cells. This fact might be reflected in the low toxic profile of ASP3026.

In intrapleural and intra-hepatic xenograft models of NOD/SCID mice with NCI-H2228 tumors, crizotinib at 30 mg/kg induced tumor regression during the initial treatment phase, but tumors then increased in size despite continuation of oral dosing of crizotinib. The plasma concentrations of crizotinib were 1.3, 1.5, and 1.3 μg/mL at 2, 4, and 8 h after 14-day repeated oral administration at 30 mg/kg in mice with intra-hepatic xenografts (data not shown). In patients with ALK fusion-positive NSCLC, the median trough concentration of crizotinib at steady state is reported to be approximately 0.3 μg/mL (45). Based on the reported clinical data, my colleagues and I consider that sufficient drug exposure was achieved in mice administered 30 mg/kg crizotinib. In the two xenograft models, treatment with 30 mg/kg ASP3026 induced continuous tumor reduction, indicating that ASP3026 has potential efficacy against metastatic lesions in patients refractory to crizotinib, although this conclusion should be re-evaluated once pharmacokinetic data in humans becomes available.

The gatekeeper-residue mutation L1196M of ALK was initially found in ALK-positive NSCLC patients who relapsed after an initial response to crizotinib (39, 46-48). In the present experiments, crizotinib exhibited 10-fold weaker inhibitory activity against EML4-ALK with L1196M compared to wild-type EML4-ALK, and no inhibitory activity was detected in a xenograft model at an oral daily dose of 100 mg/kg, as was shown in previous reports (35, 36). The inhibitory activity of ASP3026 was approximately 3-fold weaker for EML4-ALK with the L1196M mutation, but in the xenograft model, ASP3026 also induced tumor regression in cells expressing this gatekeeper-residue mutant as well as wild-type EML4-ALK. In addition, computation modeling suggested that ASP3026 fits more deeply within the ATP-binding pocket of the gatekeeper-residue mutant form of EML4-ALK than crizotinib, which might explain why ASP3026 showed more potent efficacy within the therapeutic margin compared with crizotinib.

ASP3026 induced rapid tumor regression in subcutaneous, intrapleural, and intra-hepatic NCI-H2228 xenograft and transgenic mouse models. In these models, tumors rapidly decreased in size during the first 10 days of treatment with ASP3026, but the tumor regression then slowed. In the xenograft models, tumors were detectable at the end of each treatment period, with the size of the remaining tumors exhibiting a dependence on the dose of ASP3026. When the remaining tumors were again grown and treated with ASP3026 after a washout period of 3 weeks, the tumors rapidly decreased

in size (data not shown), indicating that the remaining tumor cells are considered to retain ALK fusion kinases. Although the mechanism underlying the reduced rate of tumor regression is unknown, it is possible that alternative pathways, such as those involving other tyrosine kinases, are upregulated in the residual tumors. In patients refractory to crizotinib, the EGFR pathway is activated due to EGFR upregulation, active mutation of EGFR, and increased ligand concentrations in pleural effusion (46-48). In addition, *KIT* gene amplification and *KRAS* mutation were also found in crizotinib refractory patients, suggesting that several alternative pathways are possibly involved in the refractory response (46, 47). The findings of several preclinical studies also indicate that alternative pathways may play an important role in resistance to crizotinib. For example, several EGFR ligands, including EGF, TGF-α, and HB-EGF, triggered resistance to ALK inhibitors against ALK-dependent cells (49), and coactivation of EGFR signaling was observed in ALK inhibitor-resistant H3122 cells (50). Tanizaki and colleagues (51) also demonstrated that EGF-mediated activation of HER family signaling is associated with ALK-TKI resistance in lung cancer positive for EML4-ALK. Thus, the combination therapy of ASP3026 with inhibitors targeting alternative pathways, such as EGFR, might lead to complete tumor regression. In the preliminary experiments, NCI-2228 cells resistant to ASP3026 developed after long-term culture in the presence of 500 to 1000 nM ASP3026. Elucidation of the resistance mechanism may help determine suitable mechanism-based medicines for treating patients resistant to ASP3026.

In the present study, ASP3026 enhanced the antitumor activity of paclitaxel and pemetrexed in a NCI-H2228 subcutaneous xenograft model, but did not synergistically enhance the activity of carboplatin. Although the reason for this latter result is unknown, importantly, ASP3026 did not enhance the toxicity of these NSCLC drugs. Increasing evidence for intratumor genetic heterogeneity is accumulating, both within individual tumor biopsies and between spatially separated biopsies of the same tumor, suggesting that solid cancer is generally heterogeneous (52, 53). As patients with ALK fusion-positive tumors are also likely to have fusion-negative tumors, the combination of ASP3026 with conventional antitumor drugs may provide therapeutic benefits to patients. Notably, however, the combination of a targeted tyrosine kinase inhibitor such as ASP3026 with cytostatic anticancer agents has not yet been proven to be generally effective and further examination of patient-derived xenografts is necessary to evaluate the potential benefits of such combination therapy.

In conclusion, ASP3026 selectively inhibits ALK kinases and has high antitumor activity and tumor penetration against ALK-driven tumors, leading to prolonged survival. ASP3026 also has a wide therapeutic margin between efficacious and toxic doses, and exhibits efficacy against crizotinib-refractory tumors. Notably, combining ASP3026 with antitumor agents enhances the activity of these compounds. My colleagues and my findings demonstrate that ASP3026 functions as a novel ALK inhibitor and is expected to improve the therapeutic outcomes of cancer patients with ALK abnormality.

Tables

Table 1. Inhibitory activity of ASP3026 and crizotinib against various TKs

Kinase	% Inhibition			
	ASP3026		Crizotinib	
	0.1 μM	1 μM	0.1 μM	1 μM
ABL	9.8	57.2	51.4	92.6
ACK	100.3	101.4	22.4	77.1
ALK	99.2	102.1	101.7	100.9
ALK(F1174L)	89.6	101.4	99.9	99.8
ALK(R1275Q)	97.6	103.0	100.4	102.1
ARG	14.8	63.0	47.8	92.1
AXL	10.9	56.0	97.2	100.6
BLK	14.5	62.5	16.5	72.6
BMX	10.5	38.0	6.9	59.0
BRK	34.2	84.6	2.0	27.4
BTK	10.8	48.0	-3.5	13.4
CSK	4.3	30.3	-3.9	15.9
CTK	-0.2	2.1	1.9	3.8
DDR1	75.1	98.8	81.1	99.1
DDR2	42.8	91.7	60.4	96.0
EGFR	24.1	69.2	-7.9	3.0
EGFR(L858R)	51.7	89.8	-5.2	8.4
EGFR(L861Q)	15.8	68.4	-3.4	-0.5
EGFR(T790M)	7.1	42.3	-3.6	0.6
EGFR(T790M/L858R)	41.7	88.5	-3.2	4.9
EPHA1	59.3	93.9	90.4	100.4
EPHA2	7.2	45.0	60.9	95.0
EPHA3	-0.6	3.6	3.7	37.2
EPHA4	3.4	28.1	23.1	76.9
EPHA5	3.1	29.2	30.3	83.0
EPHA6	0.2	2.9	61.8	99.8
EPHA7	-0.4	12.3	37.1	87.9
EPHA8	-0.5	5.9	43.2	90.4
EPHB1	32.9	83.7	75.4	99.4
EPHB2	8.5	48.6	26.1	80.4
EPHB3	1.2	29.4	-1.9	6.8
EPHB4	7.5	45.9	55.3	92.6
FAK	65.8	95.8	72.6	93.9
FER	59.5	95.7	66.8	99.4
FES	42.6	90.2	64.0	97.8
FGFR1	0.9	26.6	-0.5	34.6
FGFR2	4.5	33.3	9.6	58.2
FGFR3	3.0	30.5	10.5	64.3
FGFR4	-2.5	5.1	-4.9	2.4
FGR	26.7	73.0	33.7	83.7
FLT1	4.7	12.3	11.6	70.7
FLT3	25.9	75.0	10.9	61.6
FLT4	4.3	31.6	1.3	48.6

Kinase	% Inhibition			
	ASP3026		Crizotinib	
	0.1 μM	1 μM	0.1 μM	1 μM
FMS	74.0	97.3	55.2	95.8
FRK	73.1	97.0	5.4	48.2
FYN	45.4	91.2	13.3	67.7
HCK	15.8	68.5	1.9	38.5
HER2	-3.0	-2.3	-4.4	-4.7
HER4	22.4	72.0	-1.7	1.9
IGF1R	30.9	83.8	42.2	91.1
INSR	36.2	88.0	56.4	95.6
IRR	35.4	87.7	68.5	97.9
ITK	-2.5	14.2	17.4	78.8
JAK1	-2.7	-1.5	15.7	69.1
JAK2	0.9	3.1	85.2	99.8
JAK3	2.0	3.2	30.2	84.9
KDR	1.7	6.7	6.6	57.5
KIT	4.1	18.0	-5.4	6.6
LCK	31.9	81.3	87.3	100.6
LTK	57.7	98.4	100.4	101.4
LYNa	11.9	55.6	10.0	53.6
LYNb	8.9	49.9	8.4	50.5
MER	11.8	48.5	96.6	100.5
MET	0.5	18.3	98.9	99.9
MUSK	14.8	68.8	94.3	100.6
NPM1-ALK	96.6	102.8	102.2	100.3
PDGFRa	18.0	70.0	2.6	42.3
PDGFRb	23.7	80.4	-5.1	19.5
PYK2	56.4	93.4	76.0	98.0
RET	-2.6	6.9	8.9	62.9
RON	4.6	12.2	97.1	101.9
ROS	92.4	101.5	102.2	102.1
SRC	27.9	69.7	25.1	75.0
SRM	5.9	40.7	-2.0	1.6
SYK	0.0	17.9	27.3	76.1
TEC	-2.9	14.5	-5.5	9.9
TIE2	3.2	24.8	24.9	79.8
TNK1	78.7	98.6	10.0	57.2
TRKA	-4.7	13.6	98.2	101.3
TRKB	-3.8	0.4	94.2	100.6
TRKC	2.9	1.0	93.6	100.8
TXK	5.3	16.7	11.4	58.6
TYK2	-0.1	-0.8	1.3	40.1
TYRO3	3.3	14.5	81.0	98.6
YES	70.7	98.2	24.5	75.4
ZAP70	0.2	-0.9	2.6	39.1

Inhibitory assay for a panel of tyrosine kinases was conducted using a TK-ELISA or Off-chip MSA. Percent inhibitions were determined in a single experiment.

Table 2. Inhibitory activity of ASP3026 against various tyrosine kinases.

TK	IC_{50} (nM)	
	ASP3026	Crizotinib
wt ALK	3.5	1.5
F1174L ALK	10	1.8
R1275Q ALK	5.4	2
NPM1-ALK	6.8	2
ACK	5.8	>100
AXL	>100	3.3
L858R EGFR	86	>1000
EPHA2	>1000	54
EPHA6	>1000	54
EPHB4	>1000	68
FRK	40	>1000
JAK2	>1000	11
LCK	>100	11

TK	IC_{50} (nM)	
	ASP3026	Crizotinib
LTK	61	1.8
MER	>1000	3.4
MET	>1000	1.5
MUSK	>100	9.1
RON	>1000	5.5
ROS	8.9	0.95
TNK1	26.8	>100
TRKA	>1000	3.2
TRKB	>1000	4.6
TRKC	>1000	4.4
TYRO3	>1000	20
YES	31.5	>100

Inhibitory assay for the indicated tyrosine kinases (TK) was conducted using a TK-ELISA or Off-chip MSA. IC_{50} values were determined for TKs that were inhibited by more than 50% at 100 nM in 3 individual experiments.

Table 3. Inhibition of ALK phosphorylation and signal transduction in NCI-H2228 cells by ASP3026

Treatment	pALK		pAKT		pERK		pSTAT3	
Control	100%		100%		100%		100%	
ASP3026 10 nM	70%	**	120%		101%		88%	
ASP3026 100 nM	37%	***	56%	***	54%	***	52%	***
ASP3026 1000 nM	9%	***	20%	***	36%	***	46%	***

NCI-H2228 cells were treated with ASP3026 at the indicated concentrations for 4 h, and each protein was detected by immunoblotting using specific antibodies. The numbers represent the mean percent of phosphorylated protein/total protein relative to that in vehicle-treated cells. **: $P<0.01$, ***: $P<0.001$ compared with the value of the vehicle-treated group (Dunnett's test).

Table 4. Pharmacokinetic parameters of ASP3026 after 5-day repeated oral dosing of ASP3026 in NOD/SCID mice xenografted with NCI-H2228 cells

Dose (mg/kg/day)	Plasma			Tumor			Ratio of tumor/plasma	
	C_{max} (ng/mL)	T_{max} (h)	AUC_{0-24h} (ng·h/mL)	C_{max} (ng/g)	T_{max} (h)	AUC_{0-24h} (ng·h/g)	C_{max}	AUC_{0-24h}
1	44.3	4	630	850	4	13600	19	22
3	140	4	1820	2270	4	34400	16	19
10	508	4	5990	8990	4	121000	18	20

Table 5. Inhibitory activity of ASP3026 against EML4-ALK with gatekeeper-residue mutation L1196M

Assay	Compound	IC_{50} (nM)		Ratio (L1196M/WT)
		EML4-ALK wild-type (WT)	EML4-ALK L1196M	
(A) Kinase Inhibition	ASP3026	10	32	3.2
	Crizotinib	5	51	10
(B) Growth Inhibition of 3T3 cells	ASP3026	42	163	3.9
	Crizotinib	45	413	9.2

(A) Kinase activities of EML4-ALK variant 1 kinase (wild-type) and its L1196M-mutated form were measured with HTRF® KinEASE™-TK in the presence of ASP3026 or crizotinib. Data represent IC_{50} values of the compounds against both kinases, and the ratio of IC_{50} value for mutated versus wild type EML4-ALK. (B) 3T3 cells expressing either wild-type or mutated EML4-ALK were seeded and cultured for 1 day. Cells were then treated with ASP3026 or crizotinib for two days, and viable cell numbers were determined by the CellTiter-Glo™ Luminescent Cell Viability Assay. Data represent IC_{50} values of the compounds for both cell types, and the ratio of IC_{50} value for mutant-expressing versus wild type-expressing cells.

Figures

Fig. 1. Structure and *in-vitro* ALK inhibitory activity of ASP3026. (A) Chemical structure of ASP3026. (B) Anti-proliferative activity of ASP3026 against NCI-H2228 NSCLC cells expressing EML4-ALK. The cells were seeded on spheroid plates and treated with various concentrations of ASP3026 for 5 days. Viable cell number was determined by the CellTiter-Glo^{TM} Luminescent Cell Viability Assay to assess growth inhibition and is expressed as relative light units. Each point represents the mean relative luciferase units of triplicate replicates. The data is representative of four independent experiments. (C) Inhibition of ALK phosphorylation and signal transduction in NCI-H2228 cells by ASP3026. NCI-H2228 cells were treated with ASP3026 at the indicated concentrations for 4 h, and each protein was detected by immunoblotting using specific antibodies.

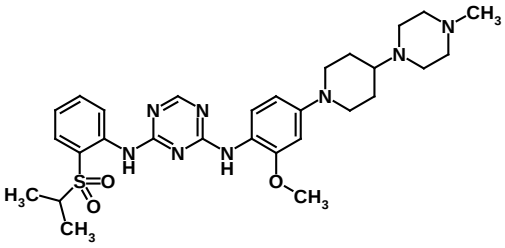

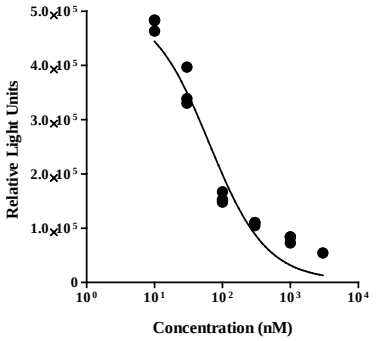
Relative Light Units
Concentration (nM)

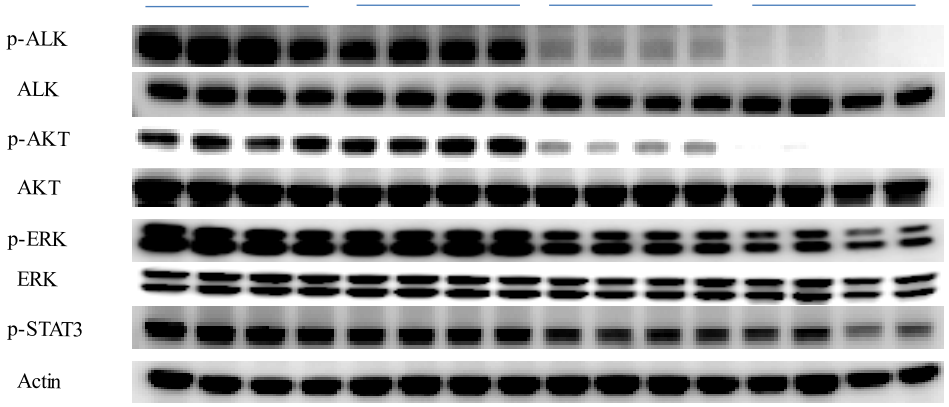
p-ALK
ALK
p-AKT
AKT
p-ERK
ERK
p-STAT3
Actin

Fig. 2. Antitumor activities of ASP3026 in a NCI-H2228 xenograft model and *hEML4-ALK* transgenic mice. (A) Inhibition of ALK phosphorylation in NCI-H2228 tumors by ASP3026. Mice with NCI-H2228 tumors were treated with ASP3026 as a single oral dose of 10 mg/kg. After 4 h, tumors were excised, and total and phosphorylated EML4-ALK were detected by immunoblotting. The numbers represent the mean percent of phosphorylated protein/total protein relative to that in the vehicle-treated group. ∗∗∗: P<0.001 compared with the value of the vehicle-treated group (Student's t-test). (B) Subcutaneously xenografted mice with NCI-H2228 cells were treated with once-daily oral administration of ASP3026 at the indicated doses for two weeks. Tumor volume and body weight were measured to assess antitumor activity. Each point represents the mean ± SEM, and the number of animals used is shown in parentheses. The values obtained on day 14 were statistically analyzed and compared. ∗∗: P<0.01 compared with the value of the control group on day 14 (Dunnett's test). (C) ASP3026 concentrations in plasma and tumors after 5-day repeated oral dosing of ASP3026 at the indicated doses in mice with NCI-H2228 tumors were measured using high-performance liquid chromatography-tandem mass spectrometry. Each point represents the mean ± SEM of three individual mice. (D) *hEML4-ALK* transgenic mice were treated with once-daily oral administration of ASP3026 at the indicated doses for 11 days. CT acquisition data were reconstructed using Inveon Acquisition Workplace software to determine tumor volume. Each point represents the mean ± SEM (n=3-4). ∗∗: P<0.01, ∗∗∗: P<0.001

compared with the value of the control group by two-way ANOVA followed by Bonferroni's multiple comparison test. n.d.: not detected.

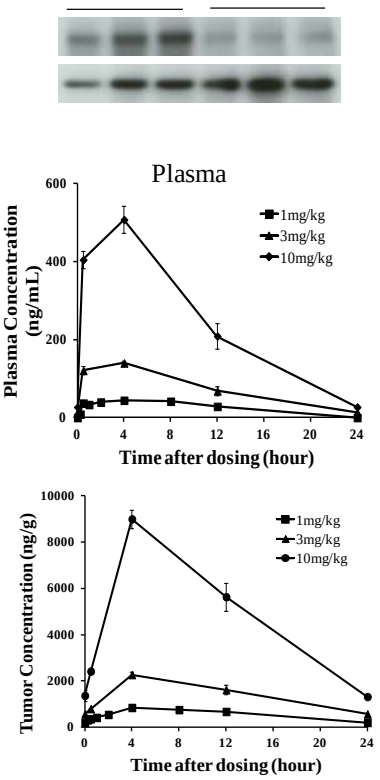

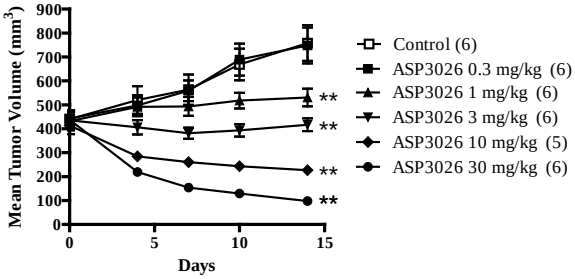

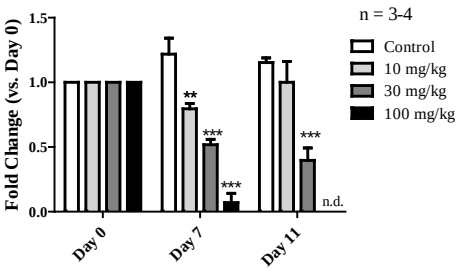

Fig. 3. Antitumor activity of twice-daily oral dosing of ASP3026 at 100 mg/kg in a NCI-H2228 xenograft model. Tumor volume (A) and body weight (B) were measured to assess antitumor activity. Each point represents the mean ± SEM (n=6). **: P<0.01 compared with the value of the control group on day 14 (Student's t-test). NS: not significant

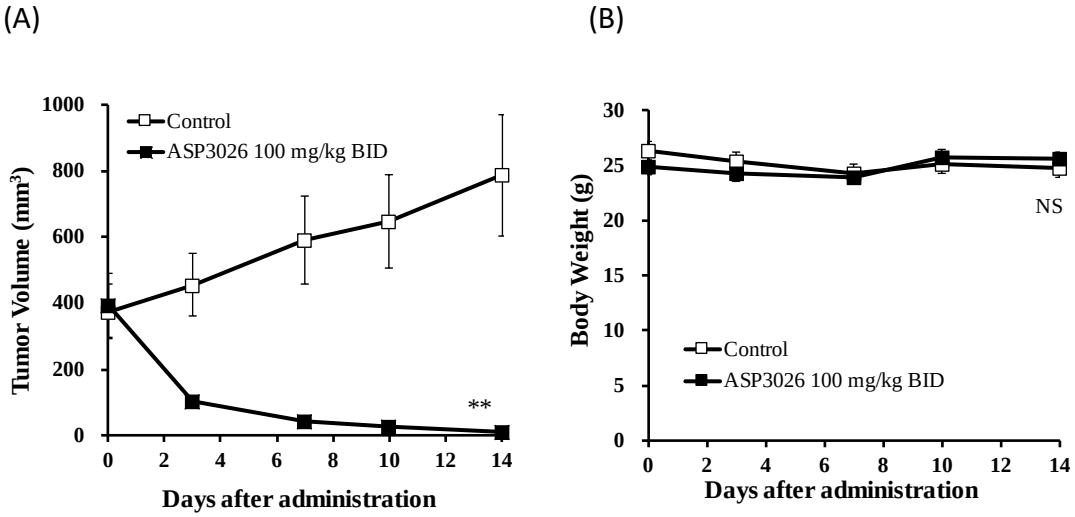

Fig. 4. Antitumor activities of ASP3026 in *hEML4-ALK* transgenic mice. *hEML4-ALK* transgenic mice were treated with once-daily oral administration of ASP3026 at the indicated doses for 11 days. The tumors were monitored by computed tomography scan.

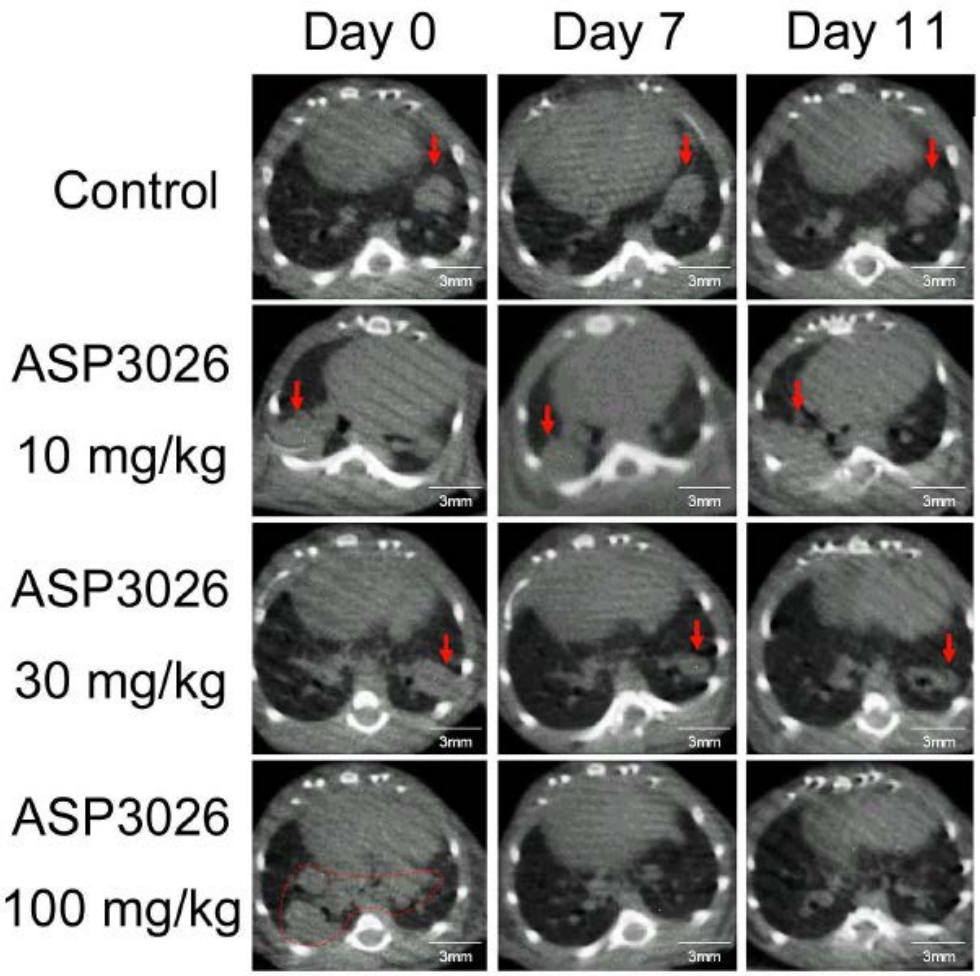

Fig. 5. Antitumor activity of ASP3026 in combination with antitumor agents against NCI-H2228 tumors. Oral ASP3026 was given once daily at 10 mg/kg in combination with (A) paclitaxel (intravenous, 12 mg/kg, days 0-4), (B) pemetrexed (intravenous, 50 mg/kg, days 0-4), or (C) carboplatin (intravenous, 60 mg/kg, days 0 and 7). Tumor volume and body weight were measured to assess antitumor activity. Each point represents the mean ± SEM (n=4-5). Values obtained on the last day of each experiment were statistically analyzed and compared. ∗: P<0.05, ∗∗: P<0.01 compared with the ASP3026 single-treatment group, +: P<0.05, ++: P<0.01 compared with each combination partner (Student's t-test). NS: not significant.

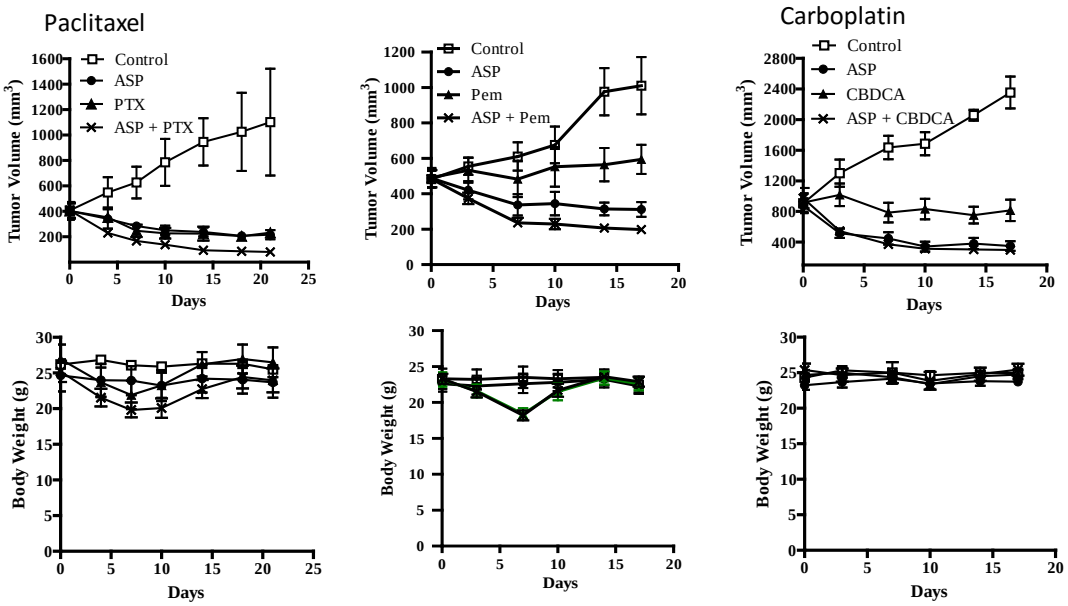

Fig. 6. Antitumor activity of ASP3026 against tumors in the pleural cavity and liver. (A) H2228-luc cells were directly inoculated into the pleural cavity of NOD/SCID mice. ASP3026 and crizotinib were orally administered once daily for 7 weeks at doses ranging from 3 to 30 mg/kg starting at 14 days after cell inoculation (n=10). The survival of mice was monitored daily, and the median survival time was determined for each group. *: $P<0.05$, **: $P<0.01$ compared with the value of the control group by the log-rank test. (B) ASP3026 and crizotinib were administered to NOD/SCID mice implanted with H2228-luc cells as in (A), and the implanted cells were monitored using BLI of the chest area. Each point represents the mean BLI ± SEM (n=8). (C) H2228-luc cells were inoculated into the portal vein of NOD/SCID mice. After confirming tumor growth, ASP3026 and crizotinib were orally administered once daily for three weeks at the indicated doses. Each point represents the mean BLI ± SEM from each animal (n=8).

(A)

Intrapleural (survival)

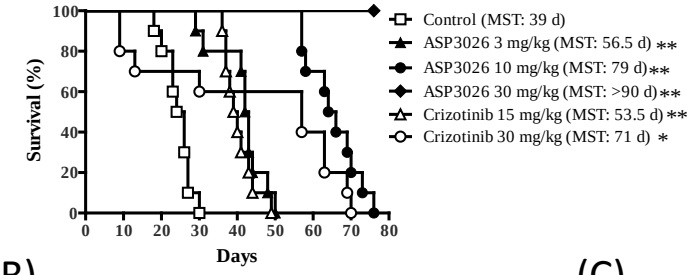

(B)

Intrapleural

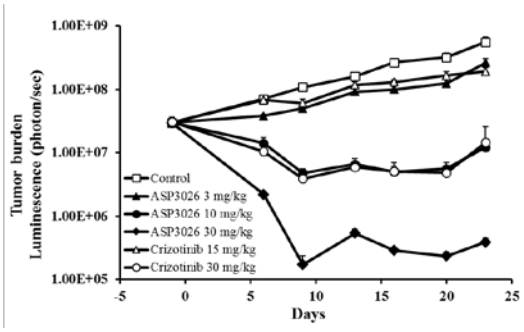

(C)

Intra-hepatic

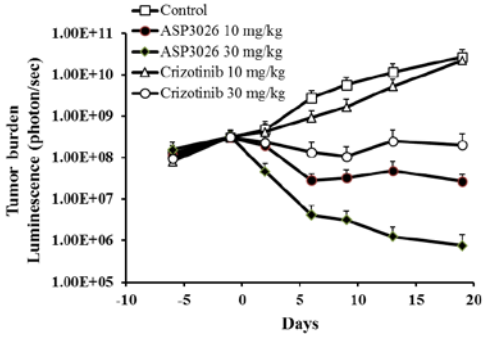

Fig. 7. Growth of H2228-luc cells directly inoculated into the pleural cavity of NOD/SCID mice. (A) The implanted cells were monitored using BLI of the chest area after luciferin injection. Each point represents the mean ± SEM (n=4-5). (B) Photographs overlayed with the imaging data at the indicated days. (C) Photographs overlayed with the imaging data from mice orally administered ASP3026 and crizotinib once daily for 23 days at the indicated doses. Dotted signals seen in control and ASP3026 10 mg/kg groups are noises in the imaging system.

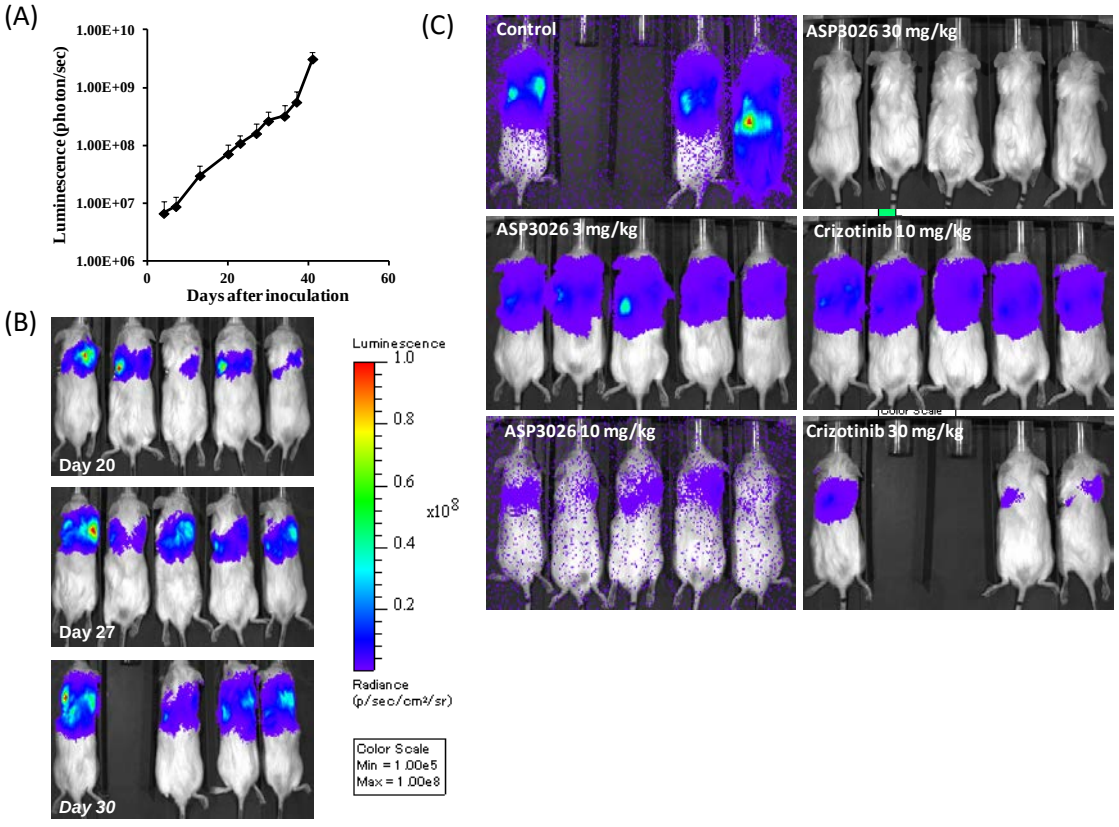

Fig. 8. Growth of H2228-luc cells in livers after inoculation into the portal vein of NOD/SCID mice. (A) The implanted cells were monitored using BLI of the abdominal area after luciferin injection. Each point represents the mean ± SEM (n=4). (B) Photographs overlayed with the imaging data at the indicated days. (C) Photographs overlayed with the imaging data from mice orally administered ASP3026 and crizotinib once daily for 19 days at the indicated doses.

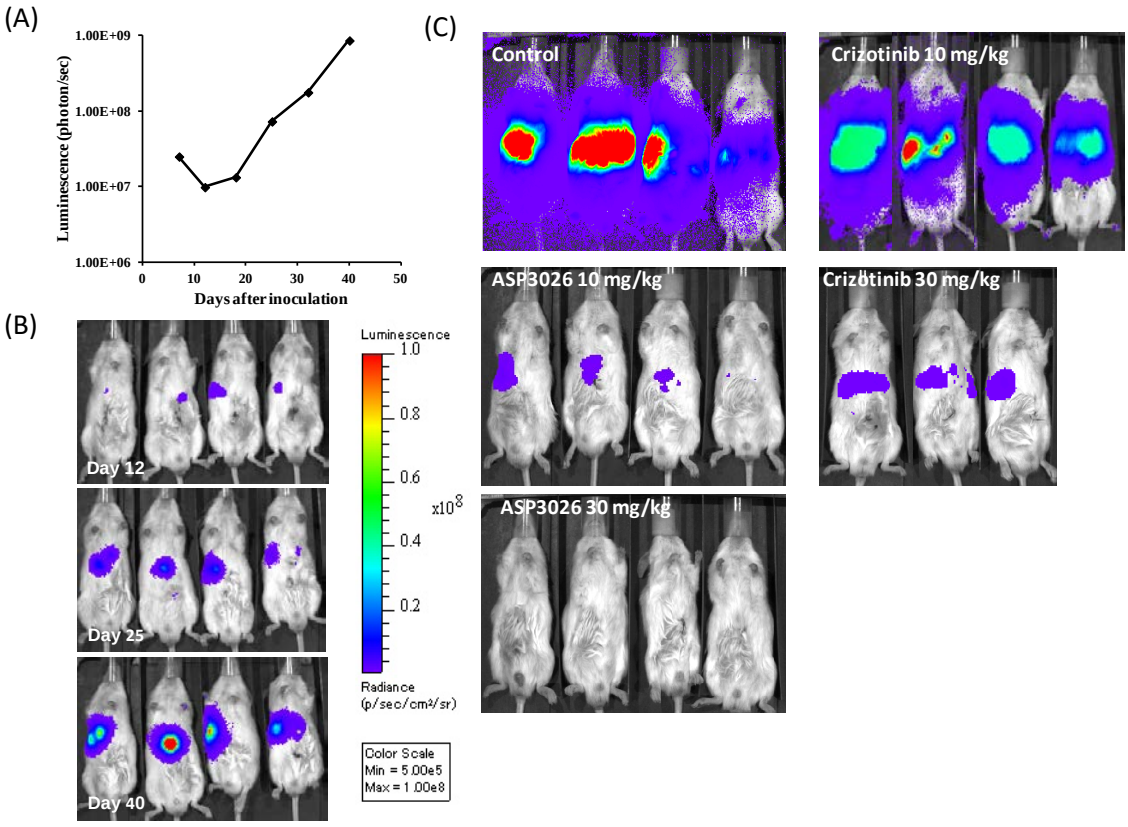

Fig. 9. Antitumor activity of ASP3026 against tumor cells expressing a gatekeeper-residue mutant of EML4-ALK, and binding modes of ASP3026 and crizotinib with wild-type and L1196M ALKs. EML4-ALK/3T3 (A) and EML4-ALK L196M/3T3 cells (B) were subcutaneously inoculated into nude mice, and ASP3026 and crizotinib were then administered to mice as a daily oral dose of 100 mg/kg/day for 5 days. Tumor volume was measured to assess antitumor activity. Each data point represents the mean ± SEM (n=4). ∗∗: $P<0.01$ compared with the value of the control group on day 5 (Dunnett's test). (C) ASP3026 and crizotinib are shown as ball-and-stick models and the gatekeeper residues (L1196 and M1196) are drawn as vdW spheres. Atoms are colored by element: white, hydrogen; cyan, carbon of ligands; gray, carbon of proteins; blue, nitrogen; red, oxygen; and yellow, sulfur). The protein surface is colored based on electrostatic potential (blue, positive; red, negative; and white, neutral). For clarity, non-polar hydrogen atoms are omitted and the protein surfaces lying anterior to the gatekeeper residues are hidden. G1202, E1210, and S1206 are potential interactive sites with the piperidine ring of crizotinib and the piperazine ring of ASP3026. The K1150 residue forms a hydrogen bond with the sulfonyl group of ASP3026.

EML4-ALK wt / 3T3

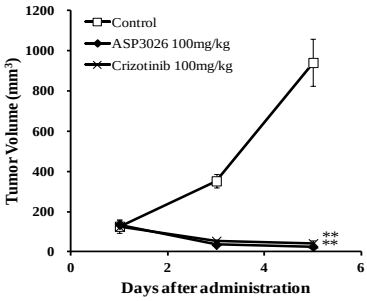

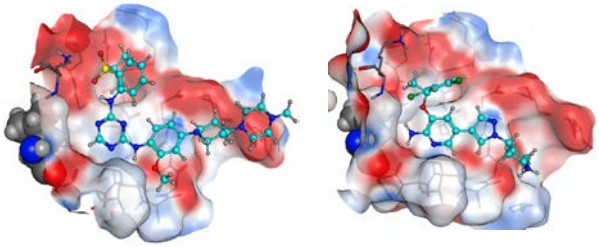

EML4-ALK L1196M/ 3T3

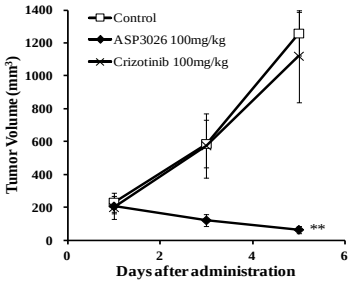

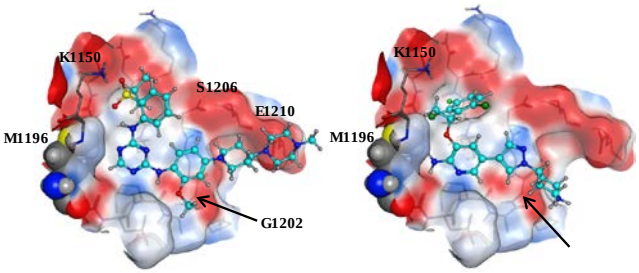

Part II

Gilteritinib, a FLT3/AXL inhibitor, shows antileukemic activity in mouse models of FLT3 mutated acute myeloid leukemia

Abstract

Advances in the understanding of the molecular basis for acute myeloid leukemia (AML) have generated new potential targets for treatment. Fms-like tyrosine kinase 3 (FLT3) is one of the most frequently mutated genes in AML and mutations in this gene are associated with poor overall survival. AXL plays a role in the activation of FLT3 and has been implicated in the pathogenesis of AML. The studies reported here evaluated the ability of a novel FLT3/AXL inhibitor, gilteritinib, to block mutated FLT3 in cellular and animal models of AML. Initial kinase studies showed that gilteritinib, a type I tyrosine kinase inhibitor, was highly selective for both FLT3 and AXL while having weak activity against c-KIT. Gilteritinib demonstrated potent inhibitory activity against the internal tandem duplication (FLT3-ITD) and FLT3-D835Y point mutations in cellular assays using MV4-11 and MOLM-13 cells as well as Ba/F3 cells expressing mutated FLT3. Gilteritinib also inhibited FLT3-F691 mutations, although to a lesser degree, in these assays. Furthermore, gilteritinib decreased the phosphorylation levels of FLT3 and its downstream targets in both cellular and animal models. *In vivo*, gilteritinib was distributed at high levels in xenografted tumors after oral administration. The decreased FLT3 activity and high intratumor distribution of gilteritinib translated to tumor regression and improved survival in xenograft and intra-bone marrow transplantation models of FLT3-driven AML. No overt toxicity was seen in mouse models treated with gilteritinib. These results indicate that gilteritinib may be an important next-generation

FLT3 inhibitor for use in the treatment of FLT3 mutation-positive AML.

Introduction

AML is a rapidly progressing hematologic cancer characterized by loss of normal differentiation and uncontrolled proliferation of hematopoietic progenitor cells in the bone marrow (54). This dysregulation of blood cell production leads to anemia, neutropenia, and thrombocytopenia (54). First-line treatment for patients (aged ≤60 years) with AML often begins with a cytarabine- and anthracycline-based chemotherapy regimen through remission induction and post-remission phases. While the complete remission rate for patients who undergo this line of treatment is over 70% (54), the 5-year survival rate is still only 50% (55). Age and leukemia cytogenetics affect patient response rate (55-58), and therapeutic outcomes are worse for patients who are not eligible for the intensive treatment or who are relapsed/refractory to front-line therapy (59, 60). A number of advances have been made in understanding the genetics behind AML (55, 56) that may lead to new opportunities for the development of targeted therapies.

FLT3 is a member of the class III receptor tyrosine kinase (TK) family that is normally expressed on the surface of hematopoietic progenitor cells (61). The FLT3 receptor plays an important role in proliferation, survival, and differentiation of multipotent stem cells (61), and mutations of FLT3 are the most common molecular alteration in AML. ITDs at the juxtamembrane domain within FLT3 are present in 25–30% of newly diagnosed AML cases (62-65), representing the most frequent FLT3-activating mutation.

Activating point mutations within the FLT3 TK domain (TKD) are also observed in patients with AML, but with less frequency than ITD mutations (64, 66). These activating mutations are oncogenic and are associated with poor prognosis, higher relapse rate, more rapid time to relapse, reduced disease-free survival, and reduced overall survival, although the prognostic impact for FLT3-TKD mutations is controversial (64-68). Overall, these findings suggest that FLT3 is a potential therapeutic target for patients with AML who are harboring a FLT3 mutation.

Similar to FLT3, AXL (a member of the TAM family of receptor TKs) has transforming properties and has been identified as a potential therapeutic target for AML (69, 70). Preclinical studies showed that inhibition of AXL blocks proliferation of FLT3 mutant and FLT3 wild-type AML cells and also suppresses the leukemic burden of FLT3-ITD^{+} AML in both a subcutaneous xenograft model and a leukemia engraftment model (69-71). Furthermore, activated AXL may be required for resistance to FLT3 inhibitors (72). Therefore, a new chemical entity that targets both FLT3 and AXL may provide a novel treatment option for AML.

Gilteritinib is a small-molecule FLT3/AXL inhibitor with a structure based on a pyrazine carboxamide scaffold. The research described here aimed at characterizing the activity of gilteritinib against FLT3-driven AML in preclinical models to elucidate the potential as an anticancer drug candidate prior to initiation of the clinical trial and also to reveal the role of the aberrant kinase in cancer biology. The inhibitory effects of

gilteritinib against FLT3 were assessed in cell-free systems and cellular assays, and its antitumor activity and survival benefits were evaluated in FLT3-driven tumors in mice.

Materials and Methods

Compounds, cell lines, and antibodies

Gilteritinib hemifumarate (referred to herein as gilteritinib), also known as ASP2215 hemifumarate, and quizartinib are small-molecule TK inhibitors (TKI) synthesized by Astellas Pharma Inc. (Tokyo, Japan). Gilteritinib and quizartinib were dissolved in DMSO or suspended in 0.5% methylcellulose for *in vitro* or *in vivo* experiments, respectively. MV4-11 cells were purchased from the American Type Culture Collection (ATCC, Manassas, VA); MOLM-13 cells were purchased from the German Collection of Microorganisms and Cell Cultures (Braunschweig, Germany). MV4-11-luc cells, which exogenously express firefly luciferase, were prepared at Astellas Pharma Inc. (a detailed protocol for the generation of the constructs is found in the online resource). MV4-11-AXL cells, which exogenously express AXL, were also prepared at Astellas Pharma Inc. Ba/F3 cells expressing FLT3-ITD, FLT3-D835Y, FLT3-ITD-D835Y, FLT3-ITD-F691L, or FLT3-ITD-F691I mutations (FLT3-ITD_Ba/F3, FLT3-D835Y_Ba/F3, FLT3-ITD-D835Y_Ba/F3, FLT3-ITD-F691L_Ba/F3, FLT3-ITD-F691I_Ba/F3) were established by Astellas Pharma Inc. The following antibodies were used for immunoblotting: FLT3 (Abcam, Cambridge, MA); phosphorylated pan-tyrosine (Merck Millipore, Billerica, MA); p44/42 MAPK (ERK1/2), phospho-p44/42 MAPK (ERK1/2) (Thr202/Tyr204) (197G2) (E10), AKT, phospho-AKT (Ser473) (193H12), and AXL (C44G1) (Cell Signaling Technology, Danvers, MA); STAT5 and phospho-STAT5

(Y694) (BD Biosciences, Franklin Lakes, NJ); phospho-AXL (Y779) (MAB6965, R&D systems, Minneapolis, MN); and β-actin (Sigma-Aldrich, St. Louis, MO).

Kinase inhibitory assays

The kinase inhibitory activity of gilteritinib was tested against a panel of 78 TKs (Table 6) using ATP concentrations that were approximately equal to the K_m value for each kinase in a TK-ELISA or off-chip mobility shift assay (MSA) at Carna Biosciences, Inc. (Kobe, Japan). These assays were conducted according to the manufacturer's instructions. Initially, two concentrations of gilteritinib (1 nM and 5 nM) were tested to assess each compound's inhibitory effect on TK activity. Further studies were then conducted using a dose range of gilteritinib to determine IC_{50} values for kinases in which activity was inhibited by >50% with 1 nM gilteritinib as well as for c-KIT. TK-ELISA and MSA assays were used to conduct IC_{50} studies for FLT3, LTK, AXL, and c-KIT; the HTRF® KinEASE™-TK assay (Sceti Medical Labo, Tokyo, Japan) was performed according to the manufacturer's protocol to assess the IC_{50} value of echinoderm microtubule-associated protein-like 4-ALK (EML4-ALK; three individual experiments for each kinase).

Cell viability assays

To examine the effect of ASP2215 on cell viability, MV4-11, MOLM-13, and Ba/F3 cells expressing either FLT3-ITD, FLT3-D835Y, FLT3-ITD-D835Y, FLT3-ITD-F691L or FLT3-ITD-F691I were seeded into 96-well white plates (Nunc F96 MicroWell™

Plates, white; Thermo Fisher Scientific Inc., Waltham, MA) at 1000 cells/well in Iscove's Modified Dulbecco's Medium, 500 cells/well in RPMI 1640 or 1000 cells/well in RPMI 1640, respectively. All cell lines were cultured overnight in a humidified incubator at 37°C with 5% CO_2 in media supplemented with 10% heat-inactivated FBS. Cell viability was determined for MV4-11 and MOLM-13 cells after 5 days of treatment with a dose course of gilteritinib; viability of Ba/F3 cells and cells expressing mutant FLT3 was assessed after treatment for 2 days with a dose course of gilteritinib and quizartinib. An additional study was conducted in Ba/F3 cells treated with both gilteritinib and IL-3 (1 ng/mL) to ascertain off-target effects of gilteritinib.

After treatment, the CellTiter-Glo® Luminescent Cell Viability Assay (Promega) was used according to the manufacturer's instructions and luminescence was measured using an ARVO-HTS plate reader (Perkin Elmer Inc., Waltham, MA). The assay was performed in either triplicate or quadruplicate. The effect of gilteritinib on cell proliferation was analyzed using SAS software (SAS Institute Inc., Cary, NC), Microsoft Excel (Microsoft), or GraphPad Prism (GraphPad Software), and the IC_{50} value of each experiment was calculated via Sigmoid-Emax model non-linear regression analysis. The geometric mean was calculated from three individual experiments.

Preparation of Ba/F3 constructs

The mutants of FLT3 (NM_004119), FLT3-D835Y (gat to tat), FLT3-ITD (insertion of acgttgatttcagagaatatgaatatgatc at 1799 position of CDS), FLT3-ITD-F691I (ttt to att),

FLT3-ITD-F691L (ttt to ctt), FLT3-ITD-D835Y were encoded into pMX-puro vector (Cell Biolabs, Inc., San Diego, CA), and transfected with FuGENE-HD (Promega) into Platinum-E cells. The next day, the culture medium was changed and cultured for 72 h, and the culture medium were recovered and filtrated. Ba/F3 cells were infected with a retroviral vector for 6 h and cultured in the growth medium for 3 days. After the drug selection with puromycin at 1.5 μg/mL for 3 days, cells were cultured in the growth medium minus IL-3.

FLT3 immunoprecipitation

For the immunoprecipitation of FLT3, MV4-11 cells were seeded into 6-well plates at 5×10^6 cells/well and cultured for 1 day prior to treatment. Following 2 h of treatment with either DMSO or a dose range of gilteritinib (0.1–10 nM), cells were lysed in RIPA buffer (Thermo Fisher Scientific) containing phosphatase and protease inhibitors, and the subsequent cell lysate was sonicated and centrifuged to pellet debris. Cell lysates (500 μg) were incubated with an anti-FLT3 antibody sc-480 (Santa Cruz Biotechnology, Santa Cruz, CA) overnight at 4°C and then incubated for 2 h with 20 μL Protein G Sepharose™ 4 Fast Flow (GE Healthcare, Fairfield, CT). The beads were washed with lysis buffer and boiled for 5 min in a 1 × SDS sample buffer (Wako Pure Chemical Industries, Osaka, Japan). Samples were electrophoresed on 7.5% gels and transferred to PVDF membranes.

Detection of downstream FLT3 targets and AXL

For the detection of ERK, STAT5, and AKT and their phosphorylated forms, MV4-11 cells were seeded at 1×10^6 cells/well in 6-well plates (AGC Techno Glass, Shizuoka, Japan) and cultured for 1 day prior to treatment with either DMSO or a dose range of gilteritinib (0.1–10 nM). Cells were treated for 2 h prior to cell lysate preparation in RIPA buffer supplemented with phosphatase and protease inhibitors. Following sample preparation, protein lysates were electrophoresed on 7.5% gels and transferred to PVDF membranes.

For the detection of AXL and phospho-AXL, MV4-11-AXL cells were seeded at 1×10^6 cells/well in 10-cm dish and cultured for 1 day prior to treatment with either DMSO or a dose range of gilteritinib (1–100 nM). Cells were treated for 4 h prior to cell lysate preparation in RIPA buffer supplemented with phosphatase and protease inhibitors. Following sample preparation, protein lysates were electrophoresed on 7.5% gels and transferred to PVDF membranes.

Immunoblotting

All membranes were blocked using either Blocking One or Blocking One-P (Nacalai Tesque Inc., Kyoto, Japan) for 1 h prior to an overnight incubation with primary antibody. Membranes were incubated overnight at 4°C with one of the following antibodies: anti-FLT3 antibody (Abcam), anti-phosphorylated pan-tyrosine, anti-ERK, anti-phospho-ERK, anti-STAT5, anti-phospho-STAT5, anti-AKT, anti-phospho-AKT, anti-AXL, anti-phospho-AXL, or anti-actin. The membranes were then washed with 1× TBS-T Buffer

and incubated with an appropriate HRP-linked secondary antibody (Cell Signaling Technology) for 1 h at room temperature. After a final wash, ECL Western Blotting Detection Reagent ECL-prime (GE Healthcare, Fairfield, CT) were applied to the membranes and signals were detected with a CCD camera (ImageQuant LAS4000; GE Healthcare). Signal intensity was then quantified using ImageQuant™ TL software (GE Healthcare). The study was performed once in triplicate, and the mean percentage of phosphorylated protein to total protein relative to that in vehicle-treated cells was calculated.

Detection of phospho-FLT3 and downstream targets in Ba/F3 cells expressing mutant FLT3.

To detect phosphorylated FLT3 and its downstream targets in Ba/F3 cells expressing mutant FLT3, cells were seeded at 6×10^6 cells per 10 cm dish and cultured overnight prior to treatment. Cells were treated with either DMSO or 0.1 nM, 1 nM, or 10 nM gilteritinib for 2 h. Cells were lysed in RIPA buffer and blotted for target proteins of interest as described earlier. Densitometry data normalized to total protein and then to the mean vehicle control for each target. Mean values reported from triplicate points.

Animal models for *in vivo* studies

All animal experimental procedures were approved by the Institutional Animal Care and Use Committee of Astellas Pharma Inc., and the Tsukuba Research Center of Astellas Pharma Inc. was awarded accreditation status by AAALAC International. Mice

were maintained on standard diet and water throughout experimental procedures.

***In vivo* mouse xenograft model**

For studies examining the *in vivo* kinase inhibitory activity of gilteritinib, male nude mice (CAnN.Cg-Foxn1nu/CrlCrlj[nu/nu]) (Charles River Laboratories Japan, Inc., Kanagawa, Japan), that were 5 weeks old, were subcutaneously inoculated with MV4-11 cells (5×10^6 cells/mouse) on day 0. After 1 month, mice were divided into groups, with each group having approximately the same mean tumor volume. Mice with MV4-11 tumors were treated with a single oral dose of gilteritinib (1 mg/kg, 3 mg/kg, 6 mg/kg, or 10 mg/kg) and tumors were excised 1 h, 2 h, 4 h, 8 h, and 24 h after administration.

For *in vivo* xenograft studies on gilteritinib antitumor activity, MV4-11 cells (5×10^6 cells/mouse) or Ba/F3 cells expressing a FLT3-ITD, FLT3-D835Y, or FLT3-ITD-D835Y mutation (3×10^6 cells/mouse) were subcutaneously injected into the flank of male nude mice at 7 weeks old (MV4-11) or 4 weeks old (Ba/F3) (Charles River Laboratories). After tumor establishment, mice were divided into groups such that the mean tumor volume was approximately equal in each group. Mice were then orally administered either 0.5% methylcellulose or once-daily gilteritinib suspended in a 0.5% methylcellulose solution at doses of 1 mg/kg, 3 mg/kg, 6 mg/kg, and 10 mg/kg (MV4-11) or 10 mg/kg and 30 mg/kg (Ba/F3).

Tumor diameter was measured using a caliper, and tumor volume was determined by calculating the volume of an ellipsoid using the formula: length × width^2 × 0.5. Body

weight was measured using a standard balance. Data are expressed as mean ± SEM from n=6 mice/group (MV4-11) and n=5 mice/group (Ba/F3).

ELISA for phosphorylated-FLT3 and total FLT3

MULTI-ARRAY® 96-well plates (Meso Scale Discovery, Rockville, MD) were coated with capture antibodies for phosphorylated FLT3 or total FLT3 (DuoSet® IC, R&D systems, Minneapolis, MN) and incubated overnight at 4°C with shaking. After washing with TBS-T, coated plates were blocked with 3% MSD® Blocker-A (Meso Scale Discovery) in TBS-T for 1 h at room temperature and then incubated with total protein lysates derived from MV4-11 xenografted tumors (500 μg/well for phosphorylated FLT3 and 20 μg/well for FLT3), overnight at 4°C. Following a wash step, anti-phosphotyrosine antibody (clone 4G10®, Biotin Conjugate [Millipore, Billerica, MA]) for the detection of phosphorylated FLT3 or the DuoSet® IC FLT3 detection antibody for total FLT3 were added to the plate and incubated for 2 h at room temperature. Wells were then washed and incubated with MSD® SULFO-TAG Labeled Streptavidin (Meso Scale Discovery) for 1 h at room temperature, followed by the addition of MSD® Read Buffer (Meso Scale Discovery). Electrochemiluminescent signals were measured using a SECTOR® imager (Meso Scale Discovery). Phosphorylation levels were normalized to total FLT3 levels in each group (3 mice/group except the point at 1 h after the administration of 1 mg/kg [2 mice]) relative to the mean value of the control group (5 mice/group). Data are reported as mean ± SEM.

Immunoblot for phosphorylated-STAT5 and STAT5 in xenograft mouse model

MV4-11 xenograft tumor protein samples were electrophoresed on 7.5% gels, transferred to PVDF membranes, and probed for phosphorylated-STAT and total STAT5 as described earlier with one alteration. Following detection of phosphorylated STAT5, the membrane was stripped using Restore™ Western Blot Stripping Buffer (Thermo Fisher Scientific) and then re-probed for total STAT5. Phosphorylation levels were normalized to total STAT5 levels in each group (3 mice/group) relative to the mean value of the control group (4 mice/group). Data are reported as mean ± SEM.

Pharmacokinetics

Nude mice subcutaneously xenografted with MV4-11 cells received gilteritinib suspended in a 0.5% methylcellulose solution as an oral single dose. Blood samples were collected at protocol-specified time points from the inferior vena cava using a syringe with EDTA-2Na, and plasma samples were prepared by centrifugation (n=3 per group; five plasma samples showed abnormal results and were not used for data analysis). Tumor samples were also collected from each mouse and tumor weight was measured. The plasma and tumor concentrations of gilteritinib were measured using high-performance liquid chromatography-tandem mass spectrometry at Nemoto Science (Ibaraki, Japan). Standard pharmacokinetic parameters (C_{max}, T_{max}, and AUC_t) were calculated from the mean concentrations of gilteritinib using WinNonlin V6.1 (Certara, Princeton, NJ).

Intra-bone marrow transplantation model

In the intra-bone marrow transplantation (IBMT) model, MV4-11-luc cells (1×10^6 cells/mouse) were injected into the bone marrow of the left tibia of female NOD-SCID mice (day 0) following the protocol detailed by Lee et al (73). Tumor growth was monitored by bioluminescent imaging of the whole body with an IVIS Spectrum (PerkinElmer, Waltham, MA). After confirming tumor cell engraftment at day 14, mice were orally administered with once-daily vehicle control or gilteritinib at 30 mg/kg from day 15 to day 70 (n=10). Tumor growth was monitored once a week during the dosing period and then every other week until day 100. Survival was also monitored daily until day 168.

Computational modeling

Docking simulation of gilteritinib with FLT3 was performed using the docking software GLIDE implemented in Maestro version 9.7 (Schrodinger, LLC, New York, NY). The coordinate of ligand–protein binding for FLT3 was modeled based on the ATP-binding form of cKIT, which had the most similar kinase domain amino acid sequence in the Protein Data Bank (PDB) (PDB ID: 1PKG, chain A) and, therefore, was used as a surrogate for FLT3. The homology modeling was done by the modeling software MOE (Chemical Computing Group Inc., Montreal, Quebec, Canada). Hydrogen atoms were added using the computer program Protonate3D implemented in MOE. The docking mode with the highest docking score was employed. All molecular visualization was

produced by MOE.

Statistical analyses

For the *in vivo* subcutaneous xenograft mouse model, values are expressed as mean ± SEM. Tumor volume and body weight on day 28 in the gilteritinib-treated groups were compared with those in the control group using Dunnett's test. For the IBMT model, the bioluminescence value on day 42 from the gilteritinib-treated group was compared with that from the control group using Student's t-test. The median survival times were compared using the log-rank test. $P<0.05$ was considered significant. SAS software (SAS Institute Inc., Cary, NC), Microsoft Excel (Microsoft, Redmond, WA), and GraphPad Prism (GraphPad Software, La Jolla, CA) were used for data processing.

Results

Gilteritinib inhibitory activity

Gilteritinib (structure provided in Fig. 10A) inhibited the activity of eight of the 78 tested kinases by over 50% at concentrations of either 1 nM (FLT3, LTK, ALK, and AXL) or 5 nM (TRKA, ROS, RET, and MER) (Table 6). The IC_{50} values were 0.29 nM for FLT3 and 0.73 nM for AXL. Gilteritinib inhibited FLT3 at an IC_{50} value that was approximately 800-fold more potent than the concentration required to inhibit c-KIT (230 nM; Table 7).

My colleagues and I next evaluated the antiproliferative activity of gilteritinib against MV4-11 and MOLM-13 cells, which endogenously express FLT3-ITD. After 5 days of treatment, gilteritinib inhibited the growth of MV4-11 and MOLM-13 cells with mean IC_{50} values of 0.92 nM (95% CI: 0.23–3.6 nM) and 2.9 nM (95% CI: 1.4–5.8 nM), respectively (Fig. 10B). Growth suppression of MV4-11 cells was accompanied by inhibition of FLT3 phosphorylation. Relative to vehicle control cells, phosphorylated FLT3 levels were 57%, 8%, and 1% after 2 h of treatment with 0.1 nM, 1 nM, and 10 nM gilteritinib, respectively (Fig. 10C). In addition, doses as low as 0.1 nM or 1 nM resulted in the suppression of phosphorylated ERK, STAT5, and AKT, all of which are downstream targets of FLT3 activation (Fig. 10D, Table 8). To investigate AXL-inhibitory activity in cells, MV4-11-AXL cells with exogenous AXL expression were treated with gilteritinib. Gilteritnib at 1 nM, 10 nM, and 100 nM for 4 h treatment

decreased the phosphorylated AXL levels to 38%, 29%, and 22%, respectively (Fig. 11).

Pharmacokinetic profile and pharmacodynamic effects of gilteritinib in an MV4-11 xenograft mouse model

The maximal plasma concentrations of gilteritinib were observed 2 h after a single oral administration of gilteritinib at 1 mg/kg, 6 mg/kg, and 10 mg/kg to MV4-11 xenografted mice. By contrast, the maximal intratumor concentrations were observed 4 h (1 mg/kg) or 8 h (6 mg/kg and 10 mg/kg) after dosing. C_{max} and AUC_t in plasma and tumors increased with increasing doses between 1 mg/kg and 10 mg/kg. The concentration in tumors was higher than that in plasma at each time point (Fig. 12A, B, Table 9).

Phosphorylated FLT3 decreased by approximately 40% compared with control phosphorylation levels in tumor samples within 1 h after single oral administration of 1–10 mg/kg gilteritinib (Fig. 12C), indicating target inhibition by gilteritinib. Although the decreased phosphorylation state observed in the 1 mg/kg treatment group had returned to the pre-treatment level by 24 h, the marked decrease in phospho-FLT3 seen with 10 mg/kg was maintained throughout the 24 h experimental period. Furthermore, the phosphorylation level of STAT5, a downstream target of FLT3, was almost completely abolished in tumors 4 h and 8 h after single administration of gilteritinib at doses of either 6 mg/kg or 10 mg/kg, respectively. STAT5 phosphorylation levels remained low 24 h post drug, approaching only 20% of baseline levels (Fig. 12D). A dose of 3 mg/kg

gilteritinib also decreased phospho-STAT5 to <20% of baseline levels at 4 h and 8 h, but returned to approximately 50% by 24 h.

The effect on tumor burden of inhibiting FLT3 phosphorylation was assessed following 28 days of once-daily oral administration of gilteritinib. Significant growth inhibition of MV4-11 tumors was observed at 1 mg/kg/day (63% inhibition; $P<0.05$) and 3 mg/kg/day (80% inhibition; $P<0.01$), and near-complete tumor regression was seen at 6 mg/kg/day (93%; $P<0.001$) and 10 mg/kg/day (100%; $P<0.001$) (Fig. 12E). Four of the six mice in the 6 mg/kg/day group experienced complete tumor regression; all six mice in the 10 mg/kg/day group experienced complete tumor regression. Body weight was not affected by treatment with gilteritinib at any tested dose (Fig. 12F).

Inhibitory activity of gilteritinib against FLT3 containing ITD ± D835Y or F691L/I mutations

Since mutations within the TKD of FLT3 (eg, FLT3-D835Y or FLT3-F691) often confer resistance to FLT3 inhibitors that were previously effective against FLT3-ITD (74), the effect of gilteritinib on these resistance mutations was studied. Gilteritinib inhibited the cell growth of Ba/F3 cells expressing either FLT3-ITD, FLT3-D835Y, FLT3-ITD-D835Y, FLT3-ITD-F691L, or FLT3-ITD-F691I, with IC_{50} values of 1.8 nM (95% CI: 1.0–3.0 nM), 1.6 nM (95% CI: 1.1–2.4 nM), 2.1 nM (95% CI: 1.4–3.0 nM), 22 nM (95% CI: 15–33 nM), and 49 nM (95% CI: 29–83 nM), respectively (Table 10). The growth of parental Ba/F3 cells in the presence of IL-3 was inhibited with an IC_{50} value

of 420 nM (95% CI: 350–500 nM), which represents the off-target inhibition of kinases other than FLT3. My colleagues and I confirmed that phosphorylation of FLT3 and its downstream targets STAT5, AKT, and ERK were inhibited by gilteritinib in a dose-dependent manner in Ba/F3 cells expressing either FLT3-ITD, FLT3-D835Y, or FLT3-ITD-D835Y (Fig. 13). Furthermore, in nude mice xenografted with Ba/F3 cells expressing either FLT3-ITD, FLT3-D835Y, or FLT3-ITD-D835Y, gilteritinib showed antitumor efficacy at 10 mg/kg and 30 mg/kg, and induced tumor regression at 30 mg/kg, in all three models (Fig. 14). As for quizartinib, 2nd generation FLT3 inhibitor, the IC50 values of growth inhibition for Ba/F3 cells expressing either FLT3-ITD, FLT3-D835Y, or FLT3-ITD-D835Y were 0.46 nM (95% CI: 0.078–2.8 nM), 5.7 nM (95% CI: 1.5–21 nM), and 35 nM (95% CI: 9.3–130 nM), respectively.

Gilteritinib binds to FLT3 at the ATP-binding site

The finding that gilteritinib inhibited FLT3-D835Y and FLT3-ITD-D835Y, both of which harbor mutations in the activation loop essential for binding type 2 inhibitors, suggests that gilteritinib is a type 1 FLT3 inhibitor. To further understand the inhibitory activity of gilteritinib against mutated FLT3 at the structural level, computational modeling was performed for FLT3 with gilteritinib (Fig. 15). The modeling revealed that gilteritinib fits into the active (DFG [Asp-Phe-Gly]-in) conformation of FLT3 at the ATP-binding site, far from the D835 position in the activation loop. The modeling also showed that gilteritinib hydrophobically interacts with FLT3 at the F691 position.

Gilteritinib prolongs survival in mice with IBMT of AML cells

Treatment with gilteritinib showed a significant reduction in overall bioluminescence, with MV4-11-luc tumor growth dramatically reduced during the first 2 weeks of treatment (Fig. 16A), resulting in bioluminescence levels that were similar to that of background (around 10^6 photons/s) on the penultimate day of treatment (day 70). Furthermore, when control mice showed MV4-11 cell infiltration in several areas of the body, gilteritinib-treated mice had no evidence of cell infiltration (Fig. 16B). Gilteritinib treatment significantly increased survival of MV4-11 xenografted mice and all treated mice survived to day 168, whereas vehicle control mice had a median survival time of 61.5 days (P<0.001) (Fig. 16C).

Discussion

These data demonstrate that gilteritinib, a FLT3/AXL TKI, shows potent efficacy in preclinical models of FLT3-mutated AML. *In vitro* kinase assays using gilteritinib revealed strong inhibition of FLT3 and AXL (in the nM range) and an 800-fold weaker inhibition of c-KIT than FLT3. Gilteritinib also inhibited phosphorylation of FLT3 with ITD and/or activation loop D835Y mutations in cellular assays. The inhibitory activity of gilteritinib against the D835Y mutation is further supported by computational modeling that showed gilteritinib binds to FLT3 within the activation loop far from the D835 site, allowing kinase inhibition to occur in the face of FLT3 mutations at this location. This potent FLT3 inhibition translated to a marked decrease in the cell viability of FLT3 mutation-positive cell lines with inhibition of several downstream targets. *In vivo*, gilteritinib was distributed at high levels in tumors after single oral administration and showed antitumor activity against FLT3-driven tumors in a mouse xenograft model. This antitumor activity was associated with a durable inhibition of phospho-FLT3 and phospho-STAT5, demonstrating the *in vivo* inhibitory effect of gilteritinib. Furthermore, treatment with gilteritinib decreased the leukemic burden and prolonged survival in a mouse IBMT model. Taken together, these data suggest that gilteritinib blocks FLT3 phosphorylation, impairs downstream signal transduction, and consequently inhibits AML cell proliferation in both *in vitro* and *in vivo* models.

These preclinical findings regarding the activity of gilteritinib suggest it may be a

potential therapeutic treatment option for patients with FLT3-mutated AML. Although several TKIs have been investigated as potential therapies for AML, none have yet to be approved for clinical use (55, 62). First-generation FLT3 inhibitors, such as sunitinib and sorafenib, are pan-kinase inhibitors that non-selectively target FLT3; this non-specificity often leads to off-target kinase inhibition and severe toxicity in patients (55). Next-generation inhibitors, such as gilteritinib, crenolanib, and quizartinib, more selectively target FLT3, suggesting less off-target effects and potentially decreased toxicity in patients. The data presented herein suggest that gilteritinib has a potent inhibitory effect on FLT3 with minimal impact on c-KIT, demonstrating the specificity of the compound. Studies have shown that mice deficient in both *flt3* and c-*kit* show a large overall decrease in hematopoietic cell number, whereas mice deficient in only *flt3* have normal mature hematopoietic populations with specific deficiencies in primitive B lymphoid progenitors (75). Thus, the targeted FLT3 inhibition and markedly weaker c-KIT inhibition by gilteritinib suggests a lower clinical risk of myelosuppression than often occurs with other TKIs (76).

When comparing the next-generation FLT3 inhibitors in development, all three compounds exhibit similar activity against FLT3-ITD *in vitro*, inhibiting the growth of MV4-11 cells at low nM concentrations (gilteritinib: 0.92 nM, crenolanib: 1.3 nM, quizartinib: 0.56 nM) (77, 78). However, gilteritinib also showed potent inhibition of FLT3-D835Y and FLT3-ITD/D835Y mutations whereas quizartinib was ineffective at

blocking these mutations (79). My colleagues and I also confirmed the weaker activity of quizartinib against FLT3-D835Y and FLT3-ITD/D835Y mutations compared to FLT3-ITD. Thus, in contrast to quizartinib, gilteritinib has the advantage of effectively blocking FLT3-ITD/D835Y and FLT3-D835Y. These preclinical data suggest that gilteritinib may provide improved clinical efficacy even in the presence of the D835Y, a mutation that has been clinically shown to confer resistance to FLT3 inhibitor treatment (80). In addition, in cellular assays, gilteritinib showed inhibitory activity against F691 mutations, a mutation also detected in patients with AML who have relapsed following quizartinib treatment (79, 81). However, in those assays, inhibition of cell viability for cells expressing FLT3-F691 was 10-fold to 20-fold weaker than for cells expressing FLT3-ITD, suggesting potential efficacy depending on the exposure level achieved in patients.

Although several similarities exist between gilteritinib and crenolanib (eg, effective inhibition of FLT3-D835Y and high selectivity for FLT3 compared with c-KIT), crenolanib treatment showed limited efficacy at the maximum tolerated dose in a xenograft mouse model in which MV4-11-luc cells were inoculated by intravenous injection, resulting in a significant survival benefit without a complete reduction in tumor cells (77). By contrast, 30 mg/kg gilteritinib induced a significant reduction in bioluminescence from tumor cells to levels near background bioluminescence and improved survival such that all mice in the gilteritinib-treatment group remained alive

during the experimental period. Furthermore, 30 mg/kg gilteritinib treatment continued to suppress the bioluminescence around 3 months post treatment, suggesting that this dose is also effective against minimum residual disease in bone marrow in this model. Overall, the cellular and animal model data suggest that gilteritinib may be advantageous compared with the other FLT3 inhibitors in development because it effectively blocks mutated FLT3 (both FLT3-ITD and FLT3-D835Y).

In addition to the strong preclinical inhibition of FLT3, gilteritinib also targets AXL. *In vitro* studies have shown that AXL is important for both wild-type and mutant FLT3 activation, suggesting that AXL may have a role in the pathobiology of AML (70). Furthermore, preclinical evidence in FLT3-ITD expressing cells suggests that activation of AXL may be required for the development of acquired resistance to FLT3 inhibitors (72). Additional *in vivo* studies have demonstrated that blocking AXL can suppress the growth of FLT3-ITD AML (70), decrease tumor size (69), and block the activation of cellular survival pathways while upregulating the apoptotic pathway (69). Thus, the preliminary preclinical data presented herein, showing that gilteritinib inhibits AXL at concentrations similar to that for FLT3, suggest that dual inhibition of this pathway may lead to improved efficacy in the treatment of AML; however, it remains unclear whether AXL inhibition played a role in the tumor regression and improved survival induced by gilteritinib in the IBMT model.

Although these preclinical studies clearly demonstrate the potent activity of

gilteritinib on FLT3 coupled with minimal activity against c-KIT, a few limitations should be noted. While these data are suggestive of a possible enhanced benefit to blocking both FLT3 and AXL, further studies are needed to fully characterize and understand the effect of gilteritinib on AXL in preclinical models thereby helping to fully elucidate the role of AXL in FLT3-mutated AML. In addition, understanding the effect of gilteritinib in cells from patients with AML may help shed light on the clinical implications of treatment with a FLT3-mutant inhibitor because the patient's cells will be heterogeneous for the FLT3 mutation.

Overall, gilteritinib showed consistently potent inhibition of FLT3 in preclinical studies and demonstrated strong efficacy in FLT3-mutant tumor models. Furthermore, initial *in vitro* assays suggest that gilteritinib effectively blocks AXL activity while having minimal effect on c-KIT. Based on these data, it can be postulated that gilteritinib may lead to a reduced blast number and prolonged survival in patients with FLT3-ITD- or FLT3-D835Y-positive AML. This hypothesis requires confirmation in clinical studies.

Tables

Table 6. Inhibitory activity of gilteritinib against various tyrosine kinases

Kinase	% inhibition		Kinase	% inhibition	
	1 nM	5 nM		1 nM	5 nM
ABL	-13.1	-10.4	HCK	-8.1	-6.6
ACK	-4.1	-2.5	HER2	-7.9	-8.9
ALK	76.1	97.6	HER4	-1.0	-6.1
ARG	-4.0	-3.7	IGF1R	6.4	24.1
AXL	54.3	85.5	INSR	10.5	37.3
BLK	-3.6	-1.0	IRR	7.2	23.4
BMX	-5.0	-4.1	ITK	-0.6	0.6
BRK	-10.0	-0.7	JAK1	-8.1	-5.5
BTK	-3.0	6.1	JAK2	-1.7	6.3
CSK	1.2	-3.1	JAK3	-0.7	7.4
DDR1	1.4	14.0	KDR	-1.6	3.1
DDR2	2.4	13.3	KIT	0.5	0.5
EGFR	0.8	1.0	LCK	-5.2	2.3
EPHA1	4.8	17.6	LTK	81.8	97.5
EPHA2	-6.9	-8.7	LYNa	-3.8	-1.4
EPHA3	-8.6	-7.4	LYNb	-3.5	-1.3
EPHA4	-6.4	-3.4	MER	21.5	55.7
EPHA5	-5.1	-8.8	MET	-0.5	5.0
EPHA6	-11.0	-9.5	MUSK	-4.9	8.5
EPHA7	-7.3	-12.0	PDGFRα	-5.4	13.0
EPHA8	-5.2	-10.3	PDGFRβ	-3.8	2.4
EPHB1	-7.1	-4.8	PYK2	-0.4	2.1
EPHB2	-6.1	-7.8	RET	26.0	65.5
EPHB3	-6.6	-10.0	RON	0.4	6.8
EPHB4	-6.0	-9.1	ROS	35.0	71.7
FAK	-5.6	-8.3	SRC	-2.1	1.6
FER	5.2	21.7	SRM	-7.3	-8.6
FES	-0.2	-0.8	SYK	-9.3	6.1
FGFR1	-5.6	-6.0	TEC	-2.2	-4.5
FGFR2	-7.0	-6.6	TIE2	-9.4	-13.5
FGFR3	-9.5	-6.9	TNK1	-1.0	5.1
FGFR4	-9.2	-7.7	TRKA	38.3	74.9
FGR	-2.3	6.0	TRKB	6.6	23.8
FLT1	-2.1	3.9	TRKC	4.7	29.9
FLT3	86.8	96.4	TXK	-2.6	-1.1
FLT4	-4.3	25.7	TYK2	-5.7	-4.5
FMS	2.1	20.0	TYRO3	-7.8	2.0
FRK	-5.1	1.1	YES	1.3	12.9
FYN	3.8	4.8	ZAP70	-5.6	-7.8

Inhibitory assay for the panel of tyrosine kinases was conducted using off-chip MSA.

Percentage inhibitions were determined in a single experiment

Table 7. Inhibitory activity of gilteritinib against various tyrosine kinases.

Kinase	IC_{50} (nmol/L)
FLT3	0.29
LTK	0.25
ALK	0.42
AXL	0.70
c-KIT	230

Inhibitory assay for the indicated tyrosine kinases (TK) was conducted using a TK-ELISA or Off-chip MSA. IC_{50} values were determined for TKs that were inhibited by more than 50% at 5 nmol/L in1 or 3 (for FLT3 and c-KIT) individual experiments.

Table 8. Gilteritinib inhibition of phosphorylated STAT5, AKT, and ERK in MV4-11 cells

Target	Kinase inhibition at the specified gilteritinib concentration (%)		
	0.1 nM	1 nM	10 nM
p-STAT5	114	23	0
p-AKT	65	48	9
p-ERK	54	22	1

Table 9. Pharmacokinetic parameters of gilteritinib after single oral dosing of gilteritinib in nude mice xenografted with MV4-11 cells

Plasma concentration		
Dose (mg/kg)	C_{max} (ng/mL)	AUC_t (ng·h/mL)
1	6.558	25.20
6	45.90	269.0
10	83.01	492.8
Intratumor concentration		
Dose (mg/kg)	C_{max} (ng/g)	AUC_t (ng·h/g)
1	90.61	1186
6	772.1	12880
10	1125	17330

AUC_t, area under the plasma concentration–time curve from time 0 h to the last determinable time point;

C_{max}, maximum plasma concentration.

Table 10. Antiproliferative activity of gilteritinib against Ba/F3 cells expressing either FLT3-ITD, FLT3-D835Y, FLT3-ITD-D835Y, FLT3-ITD-F691L or FLT3-ITD-F691I

Test compound	IC_{50} (nmol/L)					
	ITD	D835Y	ITD -D835Y	ITD -F691L	ITD -F691I	Ba/F3 IL3 (+)
Gilteritinib	1.8	1.6	2.1	22	49	420

The IC_{50} values of each experiment were calculated via Sigmoid-Emax model non-linear regression analysis. The geometric means from 3 individual experiments are shown.

Figures

Fig. 10. Gilteritinib inhibits cell growth in AML cells and blocks phosphorylation of FLT3 and its downstream targets

(A) Structure of gilteritinib (ASP2215). (B) MV4-11 and MOLM-13 cells were treated with DMSO or increasing concentrations of gilteritinib for 5 days, and cell viability was measured using CellTiter-Glo. A representative result from three independent experiments is shown. Data are presented as mean ± SEM (quadruplicate). (C) Immunoprecipitation and immunoblot for phosphorylated FLT3 and total FLT3 in MV4-11 cells treated with DMSO or increasing concentrations of gilteritinib for 2 h. Blots from one study, which was done in triplicate, are shown. Densitometry values are listed below each treatment group. (D) Immunoblot for phosphorylated AKT, ERK, and STAT5 in gilteritinib-treated MV4-11 cells. Blots from one study, which was done in triplicate, are shown.

(A)

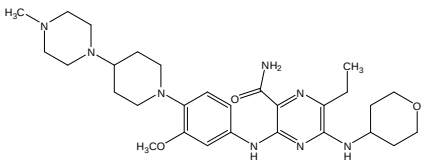

(B)

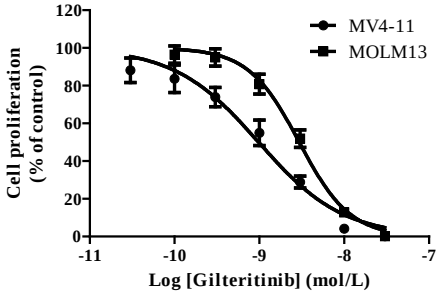
MV4-11
MOLM13
Cell proliferation
(% of control)
120
100
80
60
40
20
0
-11
-10
-9
-8
-7
Log [Gilteritinib] (mol/L)

(C)

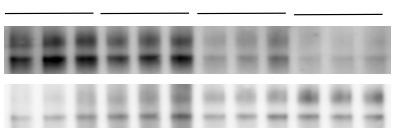

(D)

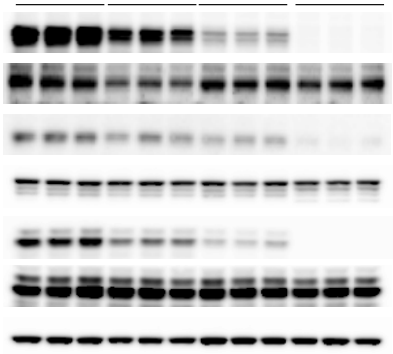

Fig. 11. Gilteritinib inhibits phosphorylation of AXL in MV4-11-AXL cells.

MV4-11-AXL cells exogenously expressing AXL were cultured overnight and treated with a dose course of gilteritinib for 4 h. Protein lysates were collected in RIPA buffer and immunoblotting was performed to detect both the phosphorylated and total form of AXL. Densitometry was performed to determine the percentage inhibition of the phosphorylated form of AXL in relation to the total protein compared with the vehicle control group. Data are presented as mean percentage inhibition; results are shown (triplicate).

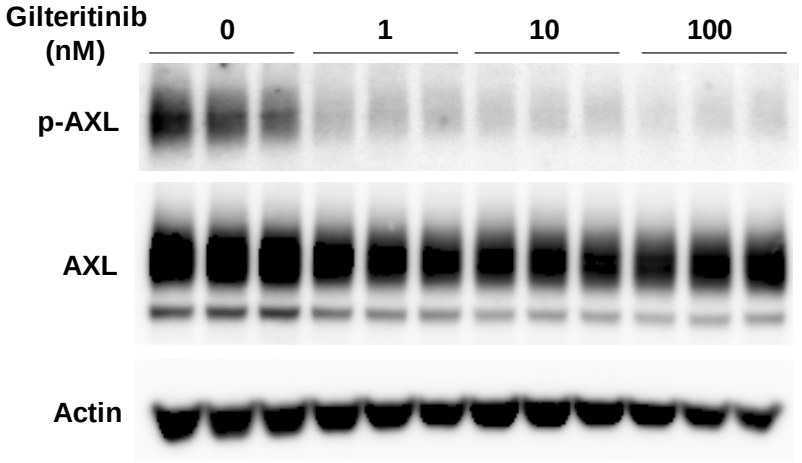

Target	Inhibition ratio		
	1 nM	10 nM	100 nM
p-AXL	62%	71%	78%

Fig. 12. Antitumor activity of gilteritinib in an MV4-11 xenograft AML mouse model

(A) Plasma concentrations of gilteritinib were determined by high-performance liquid chromatography-tandem mass spectrometry from nude mice subcutaneously xenografted with MV4-11 cells and treated with a single oral dose of gilteritinib. Data are presented as mean ± SD for two or three animals. (B) Tumor concentrations of gilteritinib were determined by high-performance liquid chromatography-tandem mass spectrometry from nude mice subcutaneously xenografted with MV4-11 cells and treated with a single dose of gilteritinib. Data are presented as mean ± SD for three animals. Symbols represent treatment groups: 1 mg/kg (●), 6 mg/kg (▲), 10 mg/kg (■). **(**C and D) Male mice xenografted with MV4-11 cells were orally treated with either vehicle control or increasing concentrations of gilteritinib. Protein lysates were collected over a 24 h time course for assessment of (C) phospho-FLT3 to total FLT3 as determined by ELISA or (D) phospho-STAT5 and total STAT5 as determined by immunoblot. Data are presented as the ratio of phosphorylated protein levels normalized to total protein levels relative to vehicle control-treated lysates. (E and F) Male mice xenografted with MV4-11 cells were orally treated with either vehicle control or increasing concentrations of gilteritinib over a 28-day period to examine the effect of drug on (E) tumor volume and (F) body weight. Data presented as mean ± SEM for n=6 mice/group. Symbols represent treatment groups: 1 mg/kg (●), 3 mg/kg (▼), 6 mg/kg (▲), 10 mg/kg (■). **P*<0.05, ***P*<0.01, and ****P*<0.001 compared with the value of the control group on Day 28

(Dunnett's test).

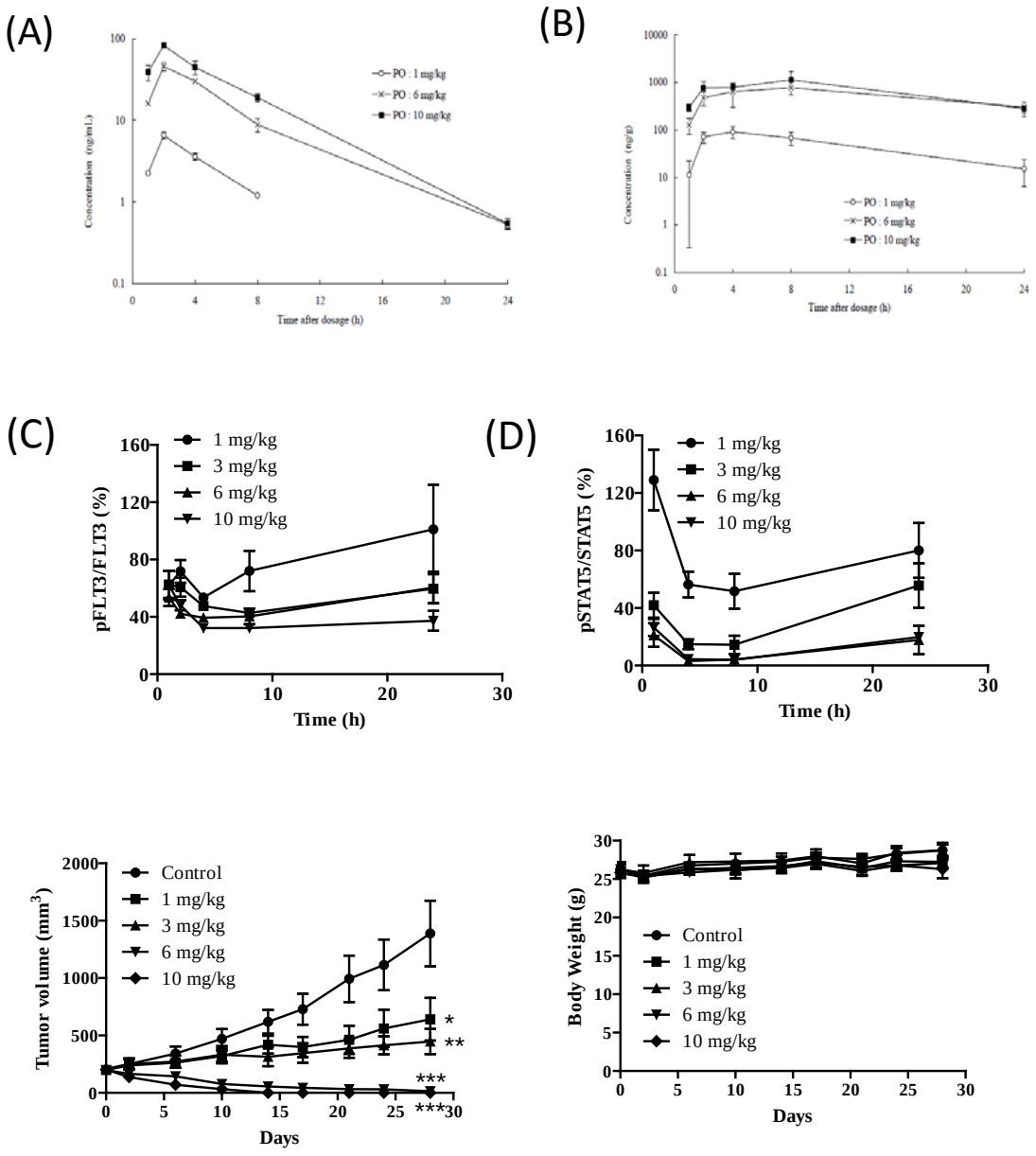

Fig. 13. Gilteritinib potently inhibits FLT3 and its downstream targets in Ba/F3 cells expressing mutant FLT3

Ba/F3 cells expressing mutant forms of FLT3 were cultured overnight and treated with a dose course of gilteritinib for 2 h. Protein lysates were collected in RIPA buffer and immunoblotting was performed to detect both the phosphorylated and total form of the target proteins FLT3, STAT5, AKT, and ERK. Immunoblot results from (A) Ba/F3 cells expressing FLT3-ITD, (B) Ba/F3 cells expressing FLT3-D835Y, (C) Ba/F3 cells expressing FLT3-ITD-D835Y. Densitometry was performed to determine the percentage inhibition of the phosphorylated form of each target in relation to the total protein compared with the vehicle control group. Data are presented as mean percentage inhibition; results are shown (triplicate)

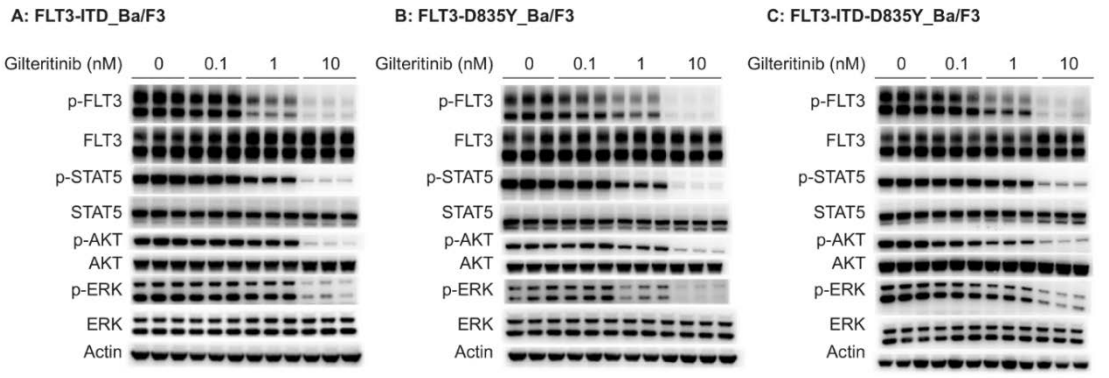

Target	Kinase inhibition at the specified gilteritinib concentration (%)		
	0.1 nM	1 nM	10 nM
p-FLT3	78	34	3
p-STAT5	99	55	5
p-AKT	81	64	5
p-ERK	93	62	10

Target	Kinase inhibition at the specified gilteritinib concentration (%)		
	0.1 nM	1 nM	10 nM
p-FLT3	74	45	1
p-STAT5	80	43	3
p-AKT	100	62	14
p-ERK	115	55	13

Target	Kinase inhibition at the specified gilteritinib concentration (%)		
	0.1 nM	1 nM	10 nM
p-FLT3	75	42	4
p-STAT5	107	86	19
p-AKT	51	27	9
p-ERK	57	40	19

Fig. 14. Gilteritinib potently inhibits FLT3 mutant-expressing tumors in a mouse xenograft model

Male nude mice were xenografted with Ba/F3 cells expressing FLT3-ITD, FLT3-D835Y, or FLT3-ITD-D835Y. Following confirmed tumor growth, mice were treated with either 10 mg/kg or 30 mg/kg once-daily oral gilteritinib for up to 7 days. Tumor volume was assessed at specified time points in (A) FLT3-ITD xenografted mice, (B) FLT3-D835Y xenografted mice, and (C) FLT3-ITD-D835Y xenografted mice. Data presented are mean ± SEM for n=5 mice/group. Symbols represent treatment groups: control (○), 10 mg/kg (■), and 30 mg/kg (♦). ***P*<0.01 and ****P*<0.001 compared with the value of the control group on Day 7 (Dunnett's test).

(A)

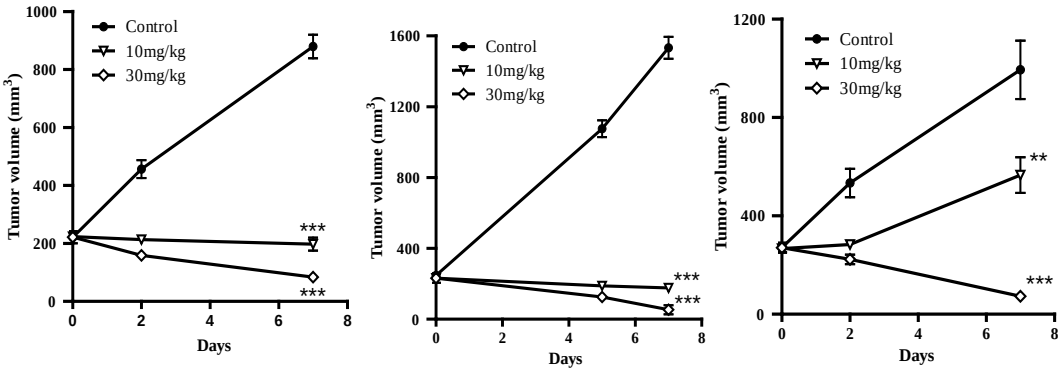

Fig. 15. Computational modeling of gilteritinib binding to wild-type FLT3

Gilteritinib is shown as a ball-and-stick model. All of atoms are colored by the type of element (white: hydrogen; cyan and gray: carbon; blue: nitrogen; red: oxygen). The protein surface is colored by electrostatic potential (blue: positive; red: negative; white: neutral). For clarity, the hydrogen atoms of the protein are omitted with the exception of the polar hydrogen atoms of the side-chains of K614 and K644; similarly, the protein surface in front of the gatekeeper residue F691 is hidden.

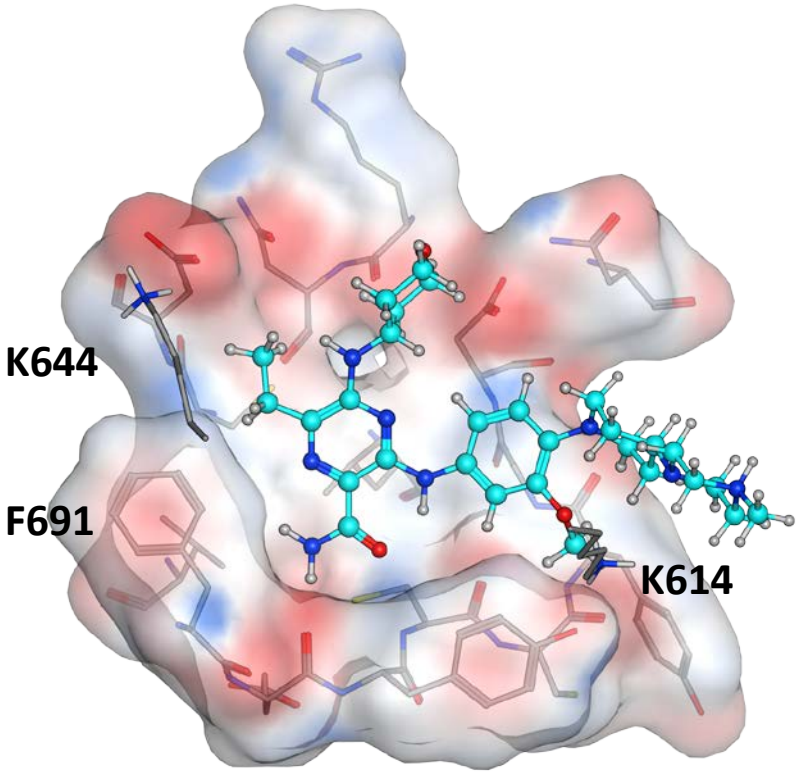

Fig. 16. Gilteritinib significantly decreases leukemic burden and increases survival in an intra-bone marrow transplantation model of AML

Female NOD-SCID mice engrafted with MV4-11-luc cells were treated once daily with vehicle (■) or 30 mg/kg gilteritinib (●) for 56 days beginning on day 15. Bar represents treatment period. (A) MV4-11-luc cell bone marrow infiltration was monitored using whole-body imaging. Data presented as mean ± SEM for n=10 mice/group. ***P<0.001 compared with the value of the control group on day 42 (Student's t-test). (B) Representative whole-body bioluminescence images from day 21 and day 42 are shown. (C) Kaplan–Meier analysis curve of mouse survival. ***P<0.001 compared with the value of the control group (Log-rank test).

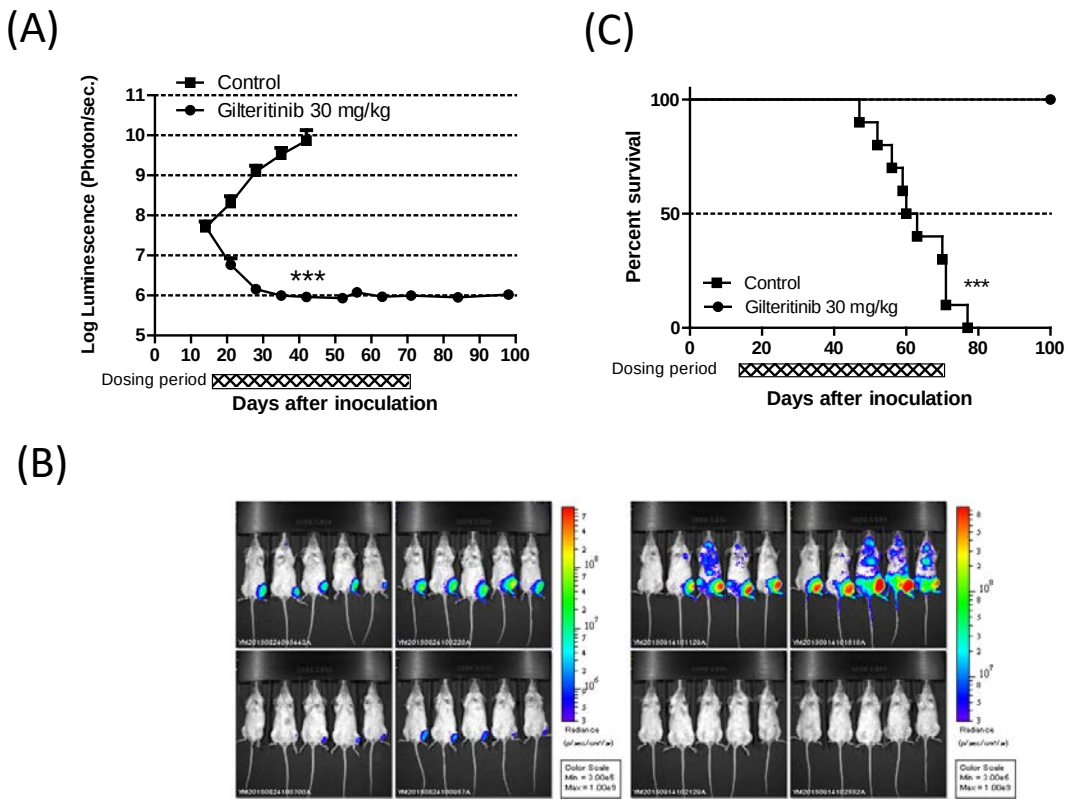

General Discussion

Gene mutation and genomic abnormality are the characteristics of cancer leading to aberrant cell growth (2-4). These alterations are the initial step for cancer development. Tumors accumulate abnormalities during their somatic evolution of life and acquire intra-tumor heterogeneity (7). When malignant cells obtain a driver mutation or genetic alteration on oncogene or tumor suppressor gene, their feature becomes more aggressive and dominant in tumor tissues. In the studies described here in this dissertation, I investigated the driver mutation dependencies of the target tumor cells harboring EML4-ALK or FLT3 with constitutively active mutation using each inhibitor, ASP3026 or gilteritinib. I also examined the basic profile of each inhibitor as an antitumor drug.

ASP3026 ALK inhibitor showed growth inhibitory activity in ALK-fusion positive NSCLC models supporting the ALK dependency of EML4-ALK positive tumor cells as assessed by previous publications (24). FLT3 dependency of FLT mutated cells was also shown in the inhibitory studies of gilteritinib in AML cells and model animals. In the report with clenoranib (82), a FLT3 inhibitor, it inhibited the cell growth of MV4-11 and MOLM14 cells with the similar potency. However, the inhibitory activities of both compounds were different among cells and/or models tested. For example, ASP3026 at 3 mg/kg induced tumor regression in mice xenografted with NCI-H2228 cells, but ASP3026 at 10 mg/kg did not induce tumor regression in the *hEML4-ALK* transgenic

mouse model although it induced regression at 30 mg/kg. The IC_{50} values of gilteritinib were 0.92 nM for the growth of MV4-11 cells, which have ITD mutation in both alleles, and 2.9 nM for that of MOLM-13 cells, which alleles consist of mutated and wild type FLT3. These findings suggest the difference in the extent of dependency in tumor cells upon each driver mutation.

Cancer dynamically evolves in its biological properties even with the treatment, and consequently acquires resistant potencies to the therapy which is often observed as appearance of treatment-resistant mutation of target molecules and/or activation of another kinase which can activate the downstream of the original target kinase (83). The ALK inhibitor crizotinib showed high efficacy in clinical trials with NSCLC patients harboring EML4-ALK, but the treatment was not curative, and the patients developed resistance to crizotinib with a progression free survival of only approximately 10 months (16-18). The gatekeeper-residue mutation L1196M of ALK was initially found in the relapsed patients (39, 46-48). In my studies, crizotinib showed no efficacy for the L1196M mutation in a xenograft model at the clinically achievable dose level. On the other hand, ASP3026 induced tumor regression in the model as well as a wild-type EML4-ALK model. In a first-in-human, open-label dose-escalation and dose-expansion study of ASP3026, its safety, pharmacokinetics, and antitumor effects were evaluated in patients with advanced solid tumors (84). Among 16 crizotinib-resistant patients with ALK positive tumors evaluated, 8 patients achieved partial response. The mean plasma

ASP3026 concentration was around 300 ng/mL (500 nM) at a steady state of 325 mg/day, the maximum tolerated dose, which was considered high enough to show the antitumor efficacy considering the nonclinical data. ASP3026 could achieve the relatively higher exposure on ALK inhibition to the extent that it inhibits the ‘gate keeper’ mutation with a tolerable safety profile compared to crizotinib in patients. This is thought to be one major reason for ASP3026 to show the efficacy against crizotinib-resistant tumors. However, the outcomes were tentative and not curative. The disease progressed over time in spite of continued treatment potentially due to tumor cells’ evolution to a treatment-resistant form in a whole organization.

ASP3026 induced rapid tumor regression in subcutaneous, intrapleural, and intra-hepatic NCI-H2228 xenograft and transgenic mouse models, but the tumors were not disappeared at the end of each treatment period. In tumors, ALK fusion positive NSCLC cells were considered to survive. In comparison with the data using ASP3026, there was one clear difference observed with gilteritinib that AML cells were disappeared by the treatment in *in vitro* and *in vivo* settings. The difference in outcomes between NSCLC cells treated with ASP3026 and AML cells treated with gilteritinib might be related to the fact AML has the lowest number of mutations among cancers (85). Although AML is not a single-gene mutated disease, its complexity of mutation is lower than solid tumors and AML tends to be sensitive to the chemo-therapies. In the clinical trial of gilteritinib in relapsed or refractory AML patients, 70 (37%) achieved composite

complete remission out of 191 FLT3 mutation-positive patients (86). On the other hand, five (9%) of 58 FLT3 wild type AML patients achieved composite complete remission. However, the outcomes seemed to be tentative and not curative also in these AML cases with gilteritinib in the preliminary analysis reported (87). Analysis of gilteritinib resistant clones revealed the acquisition of new driver mutations and selection for FLT3 wild type AML cells. My studies indicated gilteritinib had a potency to eradicate FLT3-ITD positive AML cells if efficiently exposed. Again, AML is also known to be a heterogeneous disease even in the same patient (85, 88). FLT3-ITD mutation is thought to happen in the late events of leukemogenesis. Consequently, when the blasts from FLT3 mutation-positive AML patients were analyzed for the FLT3 in a single cell polymerase chain reaction, multiple clones consisting of FLT3 wild type, FLT3-ITD/wild type, and homogeneous FLT3 ITD positive blasts were detected in the same patient. Once FLT3 is mutated to gain ITD after initiation of leukemogenesis, the blast becomes more aggressive and dominant. The malignant extent further progresses if both alleles gain the ITD mutation through loss of heterozygosity. Gilteritinib is thought to effectively reduce the number of FLT3 ITD positive blasts. But, it did not happen in all patients, and resistant clones with less FLT3 dependency appear over time as a consequence of cancer evolution with the treatment.

There are other possibilities for causes of resistance than appearance of treatment-resistant mutation of the target molecule and/or activation of another kinase which can

activate the downstream of the original target kinase (83). Recently, immuno-oncology agents, e.g. anti-programmed cell death 1 (PD1) antibody and anti-cytotoxic T lymphocyte antigen-4 (CTLA4) antibody, have shown attractive outcomes in solid tumor patients (89-91). The drugs induced complete tumor regression and the efficacies lasted for a long period in a subset of patients. Tumor cells acquire the ability to escape from immune surveillance through several ways including upregulation of immune checkpoint molecules (92). It has been proven the modification of cancer microenvironment makes tumor cells to be sensitive to immune cells at least in highly immune cell infiltrated or 'hot' tumors. The combination of ASP3026 or gilteritinib with these types of immune check point inhibitors might further improve the outcome of patients. Anyway, it is highly important to conduct real-time monitoring of tumors including microenvironment through repeated biopsies so that one can understand the current tumor biology and find appropriate treatments for the patients.

Overall, my studies revealed the basic profiles of ASP3026 and gilteritinb as molecular target therapy candidates for cancer patients, and also indicated the different dependency among tumor cells on each driver mutation with the outcomes of clinical trials. These compounds would be useful for further understanding the dramatic evolution of cancer.

Acknowledgements

I am deeply grateful for Associate Professor Kazuichi Sakamoto in Faculty of Life and Environmental Sciences, University of Tsukuba to offer valuable guidance with thoughtful advises and suggestions through my doctoral program. I also would like to express my acknowledgement to Professor Chikafumi Chiba (University of Tsukuba), Professor Satoru Kobayashi (University of Tsukuba) and Associate Professor Kentaro Nakano (University of Tsukuba) for their careful advises during the program.

Further, I would like to express my sincere thanks to Dr. Sadao Kuromitsu, Dr. Naoki Kaneko, Dr. Yoko Ueno and my colleagues in Astellas Pharma Inc. for providing opportunity of the researches and cooperating on the studies with tight discussions.

Finally, I appreciate my family to support my life with great encouragement in University of Tsukuba.

References

1. Ministry of Health, Labour and Welfare. Vital Statistics in JAPAN -The latest trends. 2016. <https://www.mhlw.go.jp/english/database/db-hw/dl/81-1a2en.pdf>
2. Miller WH Jr, Dmitrovsky E. Oncogenes and clinical oncology. Curr Opin Oncol. 1991;3:65-9.
3. Grade M, Difilippantonio MJ, Camps J. Patterns of Chromosomal Aberrations in Solid Tumors. Recent Results Cancer Res. 2015;200:115-42.
4. Schwab M, Amler LC. Amplification of cellular oncogenes: a predictor of clinical outcome in human cancer. Genes Chromosomes Cancer. 1990;1:181-93.
5. Jeggo PA, Pearl LH, Carr AM. DNA repair, genome stability and cancer: a historical perspective. Nat Rev Cancer. 2016;16:35-42.
6. Ribatti D. The concept of immune surveillance against tumors. The first theories. Oncotarget. 2017;8:7175-80.
7. McGranahan N, Swanton C. Biological and therapeutic impact of intratumor heterogeneity in cancer evolution. Cancer Cell. 2015;27:15-26.
8. Druker BJ, Sawyers CL, Kantarjian H, Resta DJ, Reese SF, Ford JM, et al. Activity of a specific inhibitor of the BCR-ABL tyrosine kinase in the blast crisis of chronic myeloid leukemia and acute lymphoblastic leukemia with the Philadelphia chromosome. N Engl J Med. 2001;344:1038-42.
9. Moen MD, McKeage K, Plosker GL, Siddiqui MA. Imatinib: a review of its use in

chronic myeloid leukaemia. Drugs. 2007;67:299-320.

10. Baselga J. Clinical trials of single-agent trastuzumab (Herceptin). Semin Oncol. 2000;5 Suppl 9:20-6.
11. Paez JG, Jänne PA, Lee JC, Tracy S, Greulich H, Gabriel S, et al. EGFR mutations in lung cancer: correlation with clinical response to gefitinib therapy. Science. 2004;304:1497-500.
12. Lynch TJ, Bell DW, Sordella R, Gurubhagavatula S, Okimoto RA, Brannigan BW, et al. Activating mutations in the epidermal growth factor receptor underlying responsiveness of non-small-cell lung cancer to gefitinib. N Engl J Med. 2004;350:2129-39.
13. Pao W, Miller V, Zakowski M, Doherty J, Politi K, Sarkaria I, et al. EGF receptor gene mutations are common in lung cancers from "never smokers" and are associated with sensitivity of tumors to gefitinib and erlotinib. Proc Natl Acad Sci U S A. 2004;101:13306-11.
14. Chapman PB, Hauschild A, Robert C, Haanen JB, Ascierto P, Larkin J, et al. Improved survival with vemurafenib in melanoma with BRAF V600E mutation. N Engl J Med. 2011;364:2507-16.
15. Fischer PM. Approved and Experimental Small-Molecule Oncology Kinase Inhibitor Drugs: A Mid-2016 Overview. Med Res Rev. 2017;37:314-67.
16. Camidge DR, Bang YJ, Kwak EL, Iafrate AJ, Varella-Garcia M, Fox SB, et al.

Activity and safety of crizotinib in patients with ALK-positive non-small-cell lung cancer: updated results from a phase 1 study. Lancet Oncol. 2012;13:1011-9.

17. Riely GJ, Evans TL, Salgia R, Ou S,. Gettinger SN, Otterson GA, et al. Results of a global phase II study with crizotinib in advanced alk-positive non-small cell lung cancer (NSCLC). 2012 Chicago Multidisciplinary Symposium in Thoracic Oncology, J Thorac Oncol. 2012;7:S204.
18. Camidge DR, Doebele RC. Treating ALK-positive lung cancer--early successes and future challenges. Nat Rev Clin Oncol. 2012;9:268-77.
19. Siegel R, Ward E, Brawley O, Jemal A. Cancer statistics, 2011: the impact of eliminating socioeconomic and racial disparities on premature cancer deaths. CA Cancer J Clin. 2011;61:212-36.
20. Janku F, Stewart DJ, Kurzrock R. Targeted therapy in non-small-cell lung cancer--is it becoming a reality? Nat Rev Clin Oncol. 2010;7:401-14.
21. Soda M, Choi YL, Enomoto M, Takada S, Yamashita Y, Ishikawa S, et al. Aburatani H, Niki T, Sohara Y, Sugiyama Y, Mano H. Identification of the transforming EML4-ALK fusion gene in non-small-cell lung cancer. Nature. 2007;448:561-6.
22. Rikova K, Guo A, Zeng Q, Possemato A, Yu J, Haack H, et al. Global survey of phosphotyrosine signaling identifies oncogenic kinases in lung cancer. Cell. 2007;131:1190-1203.
23. Takeuchi K, Choi YL, Togashi Y, Soda M, Hatano S, Inamura K, et al. KIF5B-ALK,

a novel fusion oncokinase identified by an immunohistochemistry-based diagnostic system for ALK-positive lung cancer. Clin Cancer Res. 2009;15:3143-9.

24. Soda M, Takada S, Takeuchi K, Choi YL, Enomoto M, Ueno T, et al. A mouse model for EML4-ALK-positive lung cancer. Proc Natl Acad Sci U S A. 2008;105:19893-7.

25. Chen Z, Sasaki T, Tan X, Carretero J, Shimamura T, Li D, et al. Inhibition of ALK, PI3K/MEK, and HSP90 in murine lung adenocarcinoma induced by EML4-ALK fusion oncogene. Cancer Res. 2010;70:9827-36.

26. Crystal AS, Shaw AT. New targets in advanced NSCLC: EML4-ALK. Clin Adv Hematol Oncol. 2011;9:207-14.

27. Mano H. ALKoma: a cancer subtype with a shared target. Cancer Discov. 2012;2:495-502.

28. Ladanyi M. The NPM/ALK gene fusion in the pathogenesis of anaplastic large cell lymphoma. Cancer Surv. 1997;30:59-75.

29. Lawrence B, Perez-Atayde A, Hibbard MK, Rubin BP, Dal Cin P, Pinkus JL, et al. TPM3-ALK and TPM4-ALK oncogenes in inflammatory myofibroblastic tumors. Am J Pathol. 2000;157:377-84.

30. Debelenko LV, Raimondi SC, Daw N, Shivakumar BR, Huang D, Nelson M, et al. Renal cell carcinoma with novel VCL-ALK fusion: new representative of ALK-associated tumor spectrum. Mod Pathol. 2011;24:430-42.

31. Mariño-Enríquez A, Ou WB, Weldon CB, Fletcher JA, Pérez-Atayde AR. ALK rearrangement in sickle cell trait-associated renal medullary carcinoma. Genes Chromosomes Cancer. 2011;50:146-53.

32. De Paepe P, Baens M, van Krieken H, Verhasselt B, Stul M, Simons A, et al. ALK activation by the CLTC-ALK fusion is a recurrent event in large B-cell lymphoma. Blood. 2003;102:2638-41.

33. Janoueix-Lerosey I, Lequin D, Brugières L, Ribeiro A, de Pontual L, Combaret V, et al. Somatic and germline activating mutations of the ALK kinase receptor in neuroblastoma. Nature. 2008 Oct;455:967-70.

34. Murugan AK, Xing M. Anaplastic thyroid cancers harbor novel oncogenic mutations of the ALK gene. Cancer Res. 2011;71:4403-11.

35. Sakamoto H, Tsukaguchi T, Hiroshima S, Kodama T, Kobayashi T, Fukami TA, et al. CH5424802, a selective ALK inhibitor capable of blocking the resistant gatekeeper mutant. Cancer Cell. 2011;19:679-90.

36. Lovly CM, Heuckmann JM, de Stanchina E, Chen H, Thomas RK, Liang C, et al. Insights into ALK-driven cancers revealed through development of novel ALK tyrosine kinase inhibitors. Cancer Res. 2011;71:4920-31.

37. Kwak EL, Bang YJ, Camidge DR, Shaw AT, Solomon B, Maki RG, et al. Anaplastic lymphoma kinase inhibition in non-small-cell lung cancer. N Engl J Med. 2010;363:1693-703.

38. Butrynski JE, D'Adamo DR, Hornick JL, Dal Cin P, Antonescu CR, Jhanwar SC, et al. Crizotinib in ALK-rearranged inflammatory myofibroblastic tumor. N Engl J Med. 2010;363:1727-33.

39. Choi YL, Soda M, Yamashita Y, Ueno T, Takashima J, Nakajima T, et al. ALK Lung Cancer Study Group. EML4-ALK mutations in lung cancer that confer resistance to ALK inhibitors. N Engl J Med. 2010;363:1734-9.

40. Pao W, Miller VA, Politi KA, Riely GJ, Somwar R, Zakowski MF, et al. Acquired resistance of lung adenocarcinomas to gefitinib or erlotinib is associated with a second mutation in the EGFR kinase domain. PLoS Med. 2005;2:e73.

41. Branford S, Rudzki Z, Walsh S, Grigg A, Arthur C, Taylor K, et al. High frequency of point mutations clustered within the adenosine triphosphate-binding region of BCR/ABL in patients with chronic myeloid leukemia or Ph-positive acute lymphoblastic leukemia who develop imatinib (STI571) resistance. Blood. 2002;99:3472-5.

42. Lu L, Ghose AK, Quail MR, Albom MS, Durkin JT, Holskin BP, et al. ALK Mutants in the Kinase Domain Exhibit Altered Kinase Activity and Differential Sensitivity to Small Molecule ALK Inhibitors. Biochemistry. 2009;48:3600-9.

43. Kondoh Y, Iikubo K, Kuromitsu S, Shindo N, Soga T, Furutani T, et al., inventors; Astellas Pharma Inc., et al., applicants. DI(ARYLAMINO)ARYL COMPOUND. WO 2009/008371 A1. 2009 Jan 15.

44. Galkin AV, Melnick JS, Kim S, Hood TL, Li N; Li L, et al. Identification of NVP-TAE684, a potent, selective, and efficacious inhibitor of NPM-ALK. Proc Natl Acad Sci U S A. 2007;104:270−5.

45. Tan W, Wilner KD, Bang Y, Kwak EL, Maki RG, Camidge DR, et al. Pharmacokinetics (PK) of PF-02341066, a dual ALK/MET inhibitor after multiple oral doses to advanced cancer patients. J Clin Oncol. 2010;28:abstract 2596.

46. Katayama R, Shaw AT, Khan TM, Mino-Kenudson M, Solomon BJ, Halmos B, et al. Mechanisms of acquired crizotinib resistance in ALK-rearranged lung cancers. Sci Transl Med. 2012;4:120-31.

47. Doebele RC, Pilling AB, Aisner DL, Kutateladze TG, Le AT, Weickhardt AJ, et al. Mechanisms of resistance to crizotinib in patients with ALK gene rearranged non-small cell lung cancer. Clin Cancer Res. 2012;18:1472-82.

48. Kim S, Kim TM, Kim DW, Go H, Keam B, Lee SH, et al. Heterogeneity of genetic changes associated with acquired crizotinib resistance in ALK-rearranged lung cancer. J Thorac Oncol. 2013;8:415-22.

49. Yamada T, Takeuchi S, Nakade J, Kita K, Nakagawa T, Nanjo S, et al. Paracrine receptor activation by microenvironment triggers bypass survival signals and ALK inhibitor resistance in EML4-ALK lung cancer cells. Clin Cancer Res. 2012;18:3592-602.

50. Sasaki T, Koivunen J, Ogino A, Yanagita M, Nikiforow S, Zheng W, et al. A novel

ALK secondary mutation and EGFR signaling cause resistance to ALK kinase inhibitors. Cancer Res. 2011;71:6051-60.

51. Tanizaki J, Okamoto I, Okabe T, Sakai K, Tanaka K, Hayashi H, et al. Activation of HER family signaling as a mechanism of acquired resistance to ALK inhibitors in EML4-ALK-positive non-small cell lung cancer. Clin Cancer Res. 2012;18:6219-26.
52. Swanton C. Intratumor heterogeneity: evolution through space and time. Cancer Res. 2012;72:4875-82.
53. Gerlinger M, Rowan AJ, Horswell S, Larkin J, Endesfelder D, Gronroos E, et al. Intratumor heterogeneity and branched evolution revealed by multiregion sequencing. N Engl J Med. 2012;366:883-92.
54. Estey E, Dohner H. Acute myeloid leukaemia. Lancet. 2006;368:1894–907.
55. Grunwald MR, Levis MJ. FLT3 tyrosine kinase inhibition as a paradigm for targeted drug development in acute myeloid leukemia. Semin Hematol. 2015;52:193–99.
56. Weisberg E, Boulton C, Kelly LM, Manley P, Fabbro D, Meyer T, et al. Inhibition of mutant FLT3 receptors in leukemia cells by the small molecule tyrosine kinase inhibitor PKC412. Cancer Cell. 2002;1:433–43.
57. Kantarjian H, O'Brien S, Cortes J, Giles F, Faderl S, Jabbour E, et al. Results of intensive chemotherapy in 998 patients age 65 years or older with acute myeloid

leukemia or high-risk myelodysplastic syndrome: predictive prognostic models for outcome. Cancer. 2006;106:1090–8.

58. Slovak ML, Kopecky KJ, Cassileth PA, Harrington DH, Theil KS, Mohamed A, et al. Karyotypic analysis predicts outcome of preremission and postremission therapy in adult acute myeloid leukemia: a Southwest Oncology Group/Eastern Cooperative Oncology Group Study. Blood. 2000;96:4075–83.
59. Pettit K, Odenike O. Defining and treating older adults with acute myeloid leukemia who are ineligible for intensive therapies. Front Oncol. 2015; 5:280.
60. Dombret H, Gardin C. An update of current treatments for adult acute myeloid leukemia. Blood. 2016;127:53–61.
61. Stirewalt DL, Radich JP. The role of FLT3 in haematopoietic malignancies. Nat Rev Cancer. 2003;3:650–65.
62. Pratz KW, Luger SM. Will FLT3 inhibitors fulfill their promise in acute meyloid leukemia? Curr Opin Hematol. 2014;21:72–8.
63. Nakao M, Yokota S, Iwai T, Kaneko H, Horiike S, Kashima K, et al. Internal tandem duplication of the flt3 gene found in acute myeloid leukemia. Leukemia. 1996;10:1911–8.
64. Yamamoto Y, Kiyoi H, Nakano Y, Suzuki R, Kodera Y, Miyawaki S, et al. Activating mutation of D835 within the activation loop of FLT3 in human hematologic malignancies. Blood. 2001;97:2434–9.

65. Frohling S, Schlenk RF, Breitruck J, Benner A, Kreitmeier S, Tobis K, et al. Prognostic significance of activating FLT3 mutations in younger adults (16 to 60 years) with acute myeloid leukemia and normal cytogenetics: a study of the AML Study Group Ulm. Blood. 2002;100:4372–80.

66. Abu-Duhier FM, Goodeve AC, Wilson GA, Care RS, Peake IR, Reilly JT. Identification of novel FLT-3 Asp835 mutations in adult acute myeloid leukaemia. Br J Haematol. 2001;113:983–8.

67. Bacher U, Haferlach C, Kern W, Haferlach T, Schnittger S. Prognostic relevance of FLT3-TKD mutations in AML: the combination matters--an analysis of 3082 patients. Blood. 2008;111:2527–37.

68. Whitman SP, Ruppert AS, Radmacher MD, Mrózek K, Paschka P, Langer C, et al. FLT3 D835/I836 mutations are associated with poor disease-free survival and a distinct gene-expression signature among younger adults with de novo cytogenetically normal acute myeloid leukemia lacking FLT3 internal tandem duplications. Blood. 2008;111:1552–9.

69. Ben-Batalla I, Schultze A, Wroblewski M, Erdmann R, Heuser M, Waizenegger JS et al. Axl, a prognostic and therapeutic target in acute myeloid leukemia mediates paracrine crosstalk of leukemia cells with bone marrow stroma. Blood. 2013;122:2443–52.

70. Park IK, Mishra A, Chandler J, Whitman SP, Marcucci G, Caligiuri MA. Inhibition

of the receptor tyrosine kinase Axl impedes activation of the FLT3 internal tandem duplication in human acute myeloid leukemia: implications for Axl as a potential therapeutic target. Blood. 2013;121:2064–73.

71. Janning M, Ben-Batalla I, Loges S. Axl inhibition: a potential road to a novel acute myeloid leukemia therapy? Expert Rev Hematol. 2015;8:135–8.
72. Park IK, Mundy-Bosse B, Whitman SP, Zhang X, Warner SL, Bearss DJ, et al. Receptor tyrosine kinase Axl is required for resistance of leukemic cells to FLT3-targeted therapy in acute myeloid leukemia. Leukemia. 2015;29:2382–9.
73. Lee MW, Kim HJ, Yoo KH, Kim DS, Yang JM, Kim HR, et al. Establishment of a bioluminescent imaging-based *in vivo* leukemia model by intra-bone marrow injection. Int J Oncol. 2012;41:2047–56.
74. Konig H, Levis M. Targeting FLT3 to treat leukemia. Expert Opin Ther Targets. 2015;19:37–54.
75. Mackarehtschian K, Hardin JD, Moore KA, Boast S, Goff SP, Lemischka IR. Targeted disruption of the flk2/flt3 gene leads to deficiencies in primitive hematopoietic progenitors. Immunity. 1995;3:147–61.
76. Galanis A, Levis M. Inhibition of c-Kit by tyrosine kinase inhibitors. Haematologica. 2015;100:e77–9.
77. Zimmerman EI, Turner DC, Buaboonnam J, Hu S, Orwick S, Roberts MS, et al. Crenolanib is active against models of drug-resistant FLT3-ITD-positive acute

myeloid leukemia. Blood. 2013;122:3607–15.

78. Zarrinkar PP, Gunawardane RN, Cramer MD, Gardner MF, Brigham D, Belli B, et al. AC220 is a uniquely potent and selective inhibitor of FLT3 for the treatment of acute myeloid leukemia (AML). Blood. 2009;114:2984-92.

79. Smith CC, Wang Q, Chin CS, Salerno S, Damon LE, Levis MJ, et al. Validation of ITD mutations in FLT3 as a therapeutic target in human acute myeloid leukaemia. Nature. 2012;485:260–3.

80. Smith CC, Lin K, Stecula A, Sali A, Shah NP. FLT3 D835 mutations confer differential resistance to type II FLT3 inhibitors. Leukemia. 2015;29:2390–2.

81. Smith CC, Zhang C, Lin KC, Lasater EA, Zhang Y, Massi E, et al. Characterizing and overriding the structural mechanism of the quizartinib-resistant FLT3 "Gatekeeper" F691L mutation with PLX3397. Cancer Discov. 2015;5:668–79.

82. Smith CC, Lasater EA, Lin KC, Wang Q, McCreery MQ, Stewart WK, et al. Crenolanib is a selective type I pan-FLT3 inhibitor. Proc Natl Acad Sci U S A. 2014;111:5319-24.

83. Cree IA, Charlton P. Molecular chess? Hallmarks of anti-cancer drug resistance. Due to technical constraints, your results were generated using the standard Best Match algorithm. BMC Cancer. 2017;17:10.

84. Li T, LoRusso P, Maitland ML, Ou SH, Bahceci E, Ball HA, et al. First-in-human, open-label dose-escalation and dose-expansion study of the safety,

pharmacokinetics, and antitumor effects of an oral ALK inhibitor ASP3026 in patients with advanced solid tumors. J Hematol Oncol. 2016;9:23.

85. Grove CS, Vassiliou GS. Acute myeloid leukaemia: a paradigm for the clonal evolution of cancer? Dis Model Mech. 2014;7:941-51.

86. Perl AE, Altman JK, Cortes J, Smith C, Litzow M, Baer MR. Selective inhibition of FLT3 by gilteritinib in relapsed or refractory acute myeloid leukaemia: a multicentre, first-in-human, open-label, phase 1-2 study. Lancet Oncol. 2017;18:1061-75

87. McMahon CM, Canaani J, Rea B, Sargent RL, Morrissette JJD, Lieberman DB, et al. Mechanisms of Acquired Resistance to Gilteritinib Therapy in Relapsed and Refractory FLT3 -Mutated Acute Myeloid Leukemia. Blood. 2017;130:295.

88. Stirewalt DL, Pogosova-Agadjanyan EL, Tsuchiya K, Joaquin J, Meshinchi S. Copy-neutral loss of heterozygosity is prevalent and a late event in the pathogenesis of FLT3/ITD AML. Blood Cancer J. 2014;4:e208.

89. Weber JS, D'Angelo SP, Minor D, Hodi FS, Gutzmer R, Neyns B, et al. Nivolumab versus chemotherapy in patients with advanced melanoma who progressed after anti-CTLA-4 treatment (CheckMate 037): a randomised, controlled, open-label, phase 3 trial. Lancet Oncol. 2015;16:375-84.

90. Reck M, Rodríguez-Abreu D, Robinson AG, Hui R, Csőszi T, Fülöp A, et al. Pembrolizumab versus Chemotherapy for PD-L1-Positive Non-Small-Cell Lung Cancer. N Engl J Med. 2016;375:1823-33.

91. Hodi FS, O'Day SJ, McDermott DF, Weber RW, Sosman JA, Haanen JB, et al. Improved survival with ipilimumab in patients with metastatic melanoma. N Engl J Med. 2010;363:711-23.

92. Stagg J, Johnstone RW, Smyth MJ. From cancer immunosurveillance to cancer immunotherapy. Immunol Rev. 2007;220:82-101.